MUSE IFU observations of galaxies hosting tidal disruption events

M. Pursiainen [1]*, G. Leloudas,[2] J. Lyman [1], C. M Byrne [1], P. Charalampopoulos,[3] P. Ramsden,[4,5]
S. Kim,[6] S. Schulze,[7] J. P. Anderson,[6,8] F. E. Bauer,[9] L. Dai,[10] L. Galbany,[11,12] H. Kuncarayakti,[3]
M. Nicholl [5], T. Pessi,[6] J. L. Prieto[8,13] and S. F. Sanchez [14,15]

[1]*Department of Physics, University of Warwick, Gibbet Hill Road, Coventry CV4 7AL, UK*
[2]*DTU Space, National Space Institute, Technical University of Denmark, Elektrovej 327, DK-2800 Kgs. Lyngby, Denmark*
[3]*Department of Physics and Astronomy, University of Turku, F-20014 Turku, Finland*
[4]*School of Physics and Astronomy, University of Birmingham, Birmingham B15 2TT, UK*
[5]*Astrophysics Research Centre, School of Mathematics and Physics, Queens University Belfast, Belfast BT7 1NN, UK*
[6]*European Southern Observatory, Alonso de Córdova 3107, Casilla 19, Santiago, Chile*
[7]*Center for Interdisciplinary Exploration and Research in Astrophysics (CIERA), 1800 Sherman Ave., Evanston, IL 60201, USA*
[8]*Millennium Institute of Astrophysics MAS, Nuncio Monseñor Sotero Sanz 100, Off. 104, 7500011 Providencia, Santiago, Chile*
[9]*Instituto de Alta Investigación, Universidad de Tarapacá, Casilla 7D, Arica 1030000, Chile*
[10]*Department of Physics, The University of Hong Kong, Pokfulam Road, Hong Kong, China*
[11]*Institut d'Estudis Espacials de Catalunya (IEEC), E-08034 Barcelona, Spain*
[12]*Institute of Space Sciences (ICE, CSIC), Campus UAB, Carrer de Can Magrans, s/n, E-08193 Barcelona, Spain*
[13]*Instituto de Estudios Astrofísicos, Facultad de Ingeniería y Ciencias, Universidad Diego Portales, Avenida Ejército Libertador 441, 8370191 Santiago, Chile*
[14]*Universidad Nacional Autónoma de México, Instituto de Astronomía, AP 106, Ensenada 22800, BC, Mexico*
[15]*Instituto de Astrofísica de Canarias, Vía Láctea s/n, E-38205 La Laguna, Tenerife, Spain*

ABSTRACT

We present an analysis of 20 tidal disruption events (TDEs) host galaxies observed with the Multi-Unit Spectroscopic Explorer (MUSE) integral-field spectrograph on European Southern Observatory (ESO) Very Large Telescope (VLT). We investigate the presence of extended emission line regions (EELRs) and study stellar populations mostly at sub-kpc scale around the host nuclei. EELRs are detected in 5/20 hosts, including two unreported systems. All EELRs are found at $z < 0.045$, suggesting a distance bias and faint EELRs may be missed at higher redshift. EELRs only appear in post-merger systems and all such hosts at $z < 0.045$ show them. Thus, we conclude that TDEs and galaxy mergers have a strong relation, and >45 per cent of post-merger hosts in the sample exhibit EELRs. Furthermore, we constrained the distributions of stellar masses near the central black holes (BHs), using the spectral synthesis code STARLIGHT and BPASS stellar evolution models. The youngest nuclear populations have typical ages of $\sim$1 Gyr and stellar masses below $2.5\,\mathrm{M_\odot}$. The populations that can produce observable TDEs around non-rotating BHs are dominated by sub-solar-mass stars. 3/4 TDEs requiring larger stellar masses exhibit multipeaked light curves, possibly implying relation to repeated partial disruptions of high-mass stars. The found distributions are in tension with the masses of the stars derived using light curve models. Mass segregation of the disrupted stars can enhance the rate of TDEs from supersolar-mass stars but our study implies that low-mass TDEs should still be abundant and even dominate the distribution, unless there is a mechanism that prohibits low-mass TDEs or their detection.

Key words: galaxies: starburst – galaxies: star formation – transients: tidal disruption events.

1 INTRODUCTION

When a star wanders too close to a supermassive black hole (SMBH) residing in the nucleus of a galaxy, it gets shred apart by the gravitational forces producing a bright flare. Such phenomena were first hypothesized already in the 1970s (J. G. Hills 1975), but the first tidal disruption events (TDEs) were discovered in X-rays decades later (e.g. S. Komossa & N. Bade 1999). The discoveries were rare to

begin with, but the advent of wide-field, transient surveys, such as the Sloan Digital Sky Survey (SDSS; J. E. Gunn et al. 2006), the La Silla-QUEST (LSQ; E. Hadjiyska et al. 2012), All-Sky Automated Survey for Supernovae (ASASSN; B. Shappee et al. 2014), (intermediate) Palomar Transient Factory (iPTF; N. M. Law et al. 2009), the Asteroid Terrestrial impact Last Alert System (ATLAS; J. L. Tonry et al. 2018), and the Zwicky Transient Facility (ZTF; e.g. E. C. Bellm et al. 2019), has resulted in large numbers of optically bright TDEs. Despite being discovered mostly in the optical due to the abundant surveys, TDEs are luminous in multiple wavelength regimes from radio (e.g. S. Van Velzen et al. 2016) to X-rays and γ-rays (e.g. B.

* E-mail: Miika.Pursiainen@warwick.ac.uk

A. Zauderer et al. 2011), and some are even faint in the optical with prominent emission in infrared (e.g. M. Masterson et al. 2024).

One of the early peculiarities of TDEs, was their host galaxy distribution. I. Arcavi et al. (2014) noted that their sample showed a significant preference for peculiar E+A galaxies that are otherwise passive with no significant star formation, but show strong Balmer absorption lines implying a large population of A type stars. The combination implies a strong starburst in the recent ($\lesssim 1$ Gyr) past (e.g. A. Dressler & J. E. Gunn 1983), possibly triggered by a galaxy merger (e.g. A. I. Zabludoff et al. 1996). Later studies have quantified that the overenhancement factor of TDEs in such post-starburst (PSB) galaxies to be $\gtrsim 20$ over the generic galaxy population (e.g. K. D. French, I. Arcavi & A. Zabludoff 2016; J. Law-Smith et al. 2017; O. Graur et al. 2018; E. Hammerstein et al. 2021). The TDE host galaxies also stand out photometrically. E. Hammerstein et al. (2021) notes that 63 per cent of their 19 analysed TDE hosts are found in the 'green valley' between blue star-forming galaxies, and red passive ones. The green valley is relatively bare, and the study concludes that while these galaxies represent only 13 per cent of SDSS galaxies, 61 per cent of their TDE sample is found in such galaxies indicating a clear causal relationship between TDEs and their peculiar host galaxies. Together these galaxy properties can be understood with galaxy mergers producing more concentrated central stellar distributions (e.g. E. Hammerstein et al. 2021), thus enhancing the TDE rate in these peculiar galaxies (N. C. Stone & B. D. Metzger 2016; N. C. Stone & S. v. Velzen 2016; K. D. French et al. 2020b).

The TDE hosts also often exhibit extended emission line regions (EELRs) of low velocity, non-turbulent gas that do not follow the general galaxy morphology. J. L. Prieto et al. (2016) analysed an integral field unit (IFU) data of host galaxy of ASASSN-14li taken with the Multi-Unit Spectroscopic Explorer (MUSE; R. Bacon et al. 2010) spectrograph on the Very Large Telescope (VLT), and identified significant emission of ionised [O III] $\lambda 5007$ and [N II] $\lambda 6583$ lines, extending far ($\gtrsim 10$ kpc) from the PSB host galaxy. Given the emission line strengths and widths together with the assymetric filamentry distributions of the EELRs, the study concluded that the EELRs were likely a remnant of a past merger of the galaxy hosting a weak active galactic nucleus (AGN). Similar features have since been identified in a few TDE hosts. K. D. French et al. (2023) searched for similar EELRs in a sample 93 PSB galaxies and found them in 6. Coincidentally, one of the galaxies hosted a TDE: AT 2019azh (J. T. Hinkle et al. 2021). Further, T. Wevers & K. D. French (2024) recently analysed the MUSE cube of the host of iPTF16fnl and identified prominent [O III] EELRs. The study notes that the three galaxies (of ASASSN-14li, AT 2019azh and iPTF16fnl) are all PSB galaxies and exhibit low-velocity ($\lesssim 50$ km s^{-1}) EELRs, leading to a conclusion that the post-merger host environment is crucial to understand the TDE rate. In absence of a powerful enough AGN to ionize the EELRs, they further suggest that either the EELRs are powered by frequent TDEs or that the fading AGN may be associated with increasing TDE rate or increasing rate of detecting TDEs.

One of the key TDE observables to understand, is the distribution of stars that are disrupted. The stellar masses are typically derived using light curve fitters such as Modular Open Source Fitter for Transients (MOSFIT; J. Guillochon et al. 2018) showing a distribution from $0.1\,M_\odot$ to few solar masses (see e.g. M. Nicholl et al. 2022). Furthermore, B. Mockler et al. (2022) used from *Hubble Space Telescope* (*HST*) UV spectra of three TDEs to suggest that the high nitrogen-to-oxygen abundance ratio ($N/C \geq 10$; see also C. Yang et al. 2017) of the disrupted stars is compatible only with TDEs from intermediate mass stars (1–2 $M_\odot$). As a consequence, they concluded

that TDEs from such stars are overenhanced by factor of $\gtrsim 100$ over a simple initial mass function (IMF). However, given the central SMBHs of TDE host galaxies typically have low masses ($\lesssim 10^7\,M_\odot$; e.g. P. Ramsden et al. 2022; E. Hammerstein et al. 2023b), disruption of low-mass stars is not prohibited by the Hills mass (J. G. Hills 1975), and they should produce a large number of observable TDEs. In fact, C. S. Kochanek (2016) predicted that the theoretically likeliest TDEs should be ones arising from a disruption of a $\sim 0.3\,M_\odot$ star, and TDEs from low-mass stars should dominate the population in galaxies with low-mass SMBHs. To understand the distribution of disrupted stars, a detailed spectroscopic analysis to investigate the stellar population and the stellar mass distribution in the near vicinity of the SMBH is needed.

IFU studies of supernovae (SNe) and other extragalactic transients can offer complementary constraints on the progenitors and/or explosion mechanism of individual objects of interest through characterization of their local environment within a census of their wider host galaxy properties (e.g. J. D. Lyman et al. 2020; A. J. Singleton et al. 2025). Additional power in probing progenitor channels (proxied by the stellar populations of their host galaxies) is achieved by population studies (e.g. L. Galbany et al. 2018; T. Pessi et al. 2023a), which can unveil new insights not possible without fully spatially resolved spectroscopic information (e.g. T. Pessi et al. 2023b). For TDEs, IFU observations allow to investigate the presence of the EELRs efficiently, but the data can also be used to extract volume-limited spectra of the nuclear regions needed to understand the local stellar populations. One IFU sample study of TDE host galaxies has so far been performed. E. Hammerstein et al. (2023b) analysed IFU data of 13 TDE host galaxies obtained with the Keck Cosmic Web Imager (KCWI; P. Morrissey et al. 2018), and used the high-resolution spectra to estimate the black hole masses of the hosts owning to the high spectral resolution of the instrument. Unfortunately, due to the narrow wavelength range and the small field-of-view (FoV) KCWI, the study could not investigate the presence of EELRs or touch on the stellar populations present in the nuclear regions.

In this manuscript, we present an analysis of a sample of 20 TDE host galaxies observed with MUSE, with a focus on two particular topics. The wide wavelength range 4650–9300 Å combined with the suberb spatial (0.2 arcsec px^{-1}) and wavelength resolution ($R \sim 3000$),[1] allows a detailed investigation of the EELRs characteristics, and enables determining the stellar populations in the near-vicinity of the SMBHs. The paper is structured as follows. In Section 2, we present the host sample and discuss the sample demographics, in Section 3 we investigate the presence and properties of the EELRs in the sample, and in Section 4 we determine the stellar mass distribution in the near vicinity of the SMBHs and discuss the implications for the TDEs. Finally, in Section 5, we conclude our findings.

2 SAMPLE AND OBSERVATIONS

In this paper, we analyse a sample of 20 TDE host galaxies observed with the MUSE IFU. This includes all TDE hosts that have been targeted by MUSE and are publicly available. Nine of the cubes were obtained with a dedicated programme (PI: Kim), a further nine by the all-weather MUSE supernova integral field nearby (AMUSING; L. Galbany et al. 2016; C. López-Cobá et al. 2020; Galbany et al. in preparation) survey, and two by smaller

---

[1] https://www.eso.org/sci/facilities/paranal/instruments/muse/inst.html

Table 1. TDE host galaxies observed with MUSE. Approximate date of the optical peak of the TDE, the date of MUSE observations, coordinates (J2000) spatial scale of the MUSE observation in kiloparsecs per arcsecond (kpc arcsec^{-1}) and per MUSE spaxel (kpc px^{-1}) at the redshift of each host galaxy are provided. The host galaxy types are Post-Starburst (PSB), Quiescent Balmer Strong (QBS), Quiescent (Q), and Star forming (SF) as presented in K. D. French et al. ([2016](#)), with the addition of Shocked PSB (SPOG; K. Alatalo et al. [2016](#)). The TDE spectral types are He, H+He and He following the classification scheme of S. Van Velzen et al. ([2021](#)).

TDE	Peak date	Obs. date	RA	Dec.	z	kpc arcsec^{-1}	kpc px^{-1}	Host type	Spec. type
D23H-1	2007-09-29	2019-07-28	23:31:59.54	+00:17:14.58	0.1855	3.11	0.62	SF[1]	–
PTF09axc	2009-07-23	2019-05-06	14:53:13.07	+22:14:32.2	0.1146	2.08	0.42	PSB[1]	H[2]
SDSSJ134244	2010-01-14	2019-05-06	13:42:44.42	+05:30:56.14	0.0366	0.73	0.15	SF[1]	–
LSQ12dyw[a]	2012-08-04	2021-08-16	23:29:24.87	−07:23:20.39	0.0900	1.68	0.34	SF	H[3]
ASASSN-14ae	2014-02-01	2021-03-13	11:08:40.15	+34:05:51.99	0.0436	0.86	0.17	QBS[1]	H[2]
ASASSN-14ko	2014-07-23	2015-12-02	05:25:18.12	−46:00:20.52	0.0425	0.84	0.17	SF	–
ASASSN-14li	2014-12-04	2016-01-21	12:48:15.23	+17:46:26.45	0.0206	0.42	0.08	PSB[1]	H+He[2]
iPTF15af[a]	2015-01-15	2021-02-09	08:48:28.15	+22:03:33.52	0.0790	1.49	0.30	QBS[1]	H+He[2]
ASASSN-15lh	2015-06-05	2016-08-11	22:02:15.42	−61:39:34.99	0.2326	3.71	0.74	Q	–
ASASSN-15oi	2015-08-14	2019-05-06	20:39:09.14	−30:45:20.60	0.0484	0.95	0.19	QBS[1]	He[2]
iPTF16fnl[a]	2016-09-01	2021-08-16	00:29:57.04	+32:53:37.19	0.0163	0.33	0.07	PSB[1]	H+He[2]
AT2017eqx[a]	2017-06-17	2021-09-30	22:26:48.39	+17:08:51.95	0.1089	1.99	0.40	PSB[4]	H+He[2]
AT2018dyb	2018-08-10	2019-04-12	16:10:58.87	−60:55:24.3	0.0180	0.37	0.07	Q[5]	H+He[2]
AT2018fyk	2018-09-08	2019-06-10	22:50:16.09	−44:51:53.5	0.0590	1.14	0.23	Q[6]	H+He[2]
AT2018hyz	2018-11-07	2021-02-05	10:06:50.87	+01:41:34.05	0.0458	0.90	0.18	QBS/PSB[7]	H+He[8]
AT2019ahk	2019-03-04	2019-09-02	07:00:11.39	−66:02:24.7	0.0262	0.53	0.10	SPOG[9]	H[2]
AT2019dsg[a]	2019-05-14	2021-08-05	20:57:02.96	+14:12:16.44	0.0501	0.98	0.20	SF	H+He[8]
AT2019lwu[a]	2019-07-30	2021-09-30	23:11:12.30	−01:00:10.71	0.1170	2.12	0.42	QBS/PSB	H[7]
AT2019qiz[a]	2019-10-07	2021-02-08	04:46:37.87	−10:13:34.71	0.0151	0.31	0.06	SF	H+He[8]
AT2023clx	2023-02-22	2021-03-05	11:40:09.44	+15:19:39.03	0.0111	0.23	0.05	SF	H+He[10]

Note. [a] Obtained with adaptive optics. References: (1) K. D. French et al. ([2020a](#)), (2) S. van Velzen et al. ([2020](#)), (3) P. Charalampopoulos et al. ([2022](#)), (4) M. Nicholl et al. ([2019](#)), (5) G. Leloudas et al. ([2019](#)), (6) T. Wevers et al. ([2019](#)), (7) P. Short et al. ([2020](#)), (8) E. Hammerstein et al. ([2023a](#)), (9) T. W.-S. Holoien et al. ([2019](#)) , (10) J. Zhu et al. ([2023](#)).

programmes. Seven host galaxies in our dedicated programme were observed with the adaptive optics mode, improving both the spatial resolution and the signal to noise ratio (S/N) of the observations. The cubes of ASASSN-14ko (M. A. Tucker et al. [2021](#)), ASASSN-15lh (T. Krühler et al. [2018](#)), ASASSN-14li (J. L. Prieto et al. [2016](#)), iPTF16fnl (T. Wevers & K. D. French [2024](#)), AT 2018fyk (T. Wevers et al. [2023](#)), and AT 2019qiz (Y. Xiong et al. [2025](#)) have been previously analysed in the literature. We used the default reductions provided by European Southern Observatory (ESO) for all data cubes. The data have been corrected for Galactic extinction using (E. F. Schlafly & D. P. Finkbeiner [2011](#)) reddening maps assuming $R_V = 3.1$. Throughout this paper, we assume a flat Lambda cold dark matter (ΛCDM) cosmology with $\Omega_M = 0.3$ and $H_0 = 70$ km s^{-1} Mpc^{-1}. The sample is summarized in Table [1](#), and colour images generated based on the MUSE cubes are shown in Fig. [A1](#).

We note that the sample includes two events that are outliers in the TDE populations in terms of their optical properties. First, ASASSN-14ko exhibits repeated flares from the nucleus of a merging galaxy system (e.g. A. V. Payne et al. [2021](#)). While atypical, the event can be understood as a repeating partial TDE, where the star would be partially stripped at roughly constant intervals as it passes through an AGN disc (e.g. A. V. Payne et al. [2021](#); I. Linial & E. Quataert [2023](#)), and thus we have included the event in our sample. On the other hand, ASASSN-15lh is one of the most remarkable optical transients in recent years, reaching a peak luminosity of $M_V = -23.5$. The event has been discussed both as a superluminous supernova (SLSN; S. Dong et al. [2016](#)) and a TDE (G. Leloudas et al. [2017](#)). However, the TDE classification is supported based on its host galaxy properties. ASASSN-15lh is spatially coincident with the nucleus of a galaxy hosting a massive SMBH ($M_{BH} \sim 5 \times 10^8$ M$_\odot$; T. Krühler et al.

[2018](#)), and further the galaxy does not host notable young stellar populations required for a stripped massive star progenitor of an SLSN (e.g. R. Lunnan et al. [2014](#); G. Leloudas et al. [2015](#); T. Krühler et al. [2018](#); S. Schulze et al. [2018](#)). As such, we consider ASASSN-15lh a TDE and include it in our sample.

2.1 Sample demographics

Given the MUSE data were obtained by a number of different ESO programmes, some targeting individual host galaxies and some samples of hosts, it is important to verify how representative the sample is. To investigate this, we compare the demographics of the sample with K. D. French et al. ([2020a](#), see also K. Auchettl, J. Guillochon & E. Ramirez-Ruiz [2017](#)). The work included all 41 identified TDEs with pre-TDE host spectroscopy available at the time, and offers the best comparison sample to date, in the absence of a large representative TDE host study. The hosts are labelled Post-Starburst (PSB), Quiescent Balmer Strong (QBS), Quiescent, and 'Star-forming' (SF), based on the Balmer emission/absorption line strengths in their nuclear spectra. Galaxies that show strong H δ absorption are classified as QBS (Lick H$\delta_A > 1.31$ Å) or PSB (H$\delta_A - \sigma(H\delta_A) > 4$ Å). Those that show strong H α emission (EW < -3 Å[2]) are labelled as SF galaxies, but note that as the classification relates solely to H α emission in a nuclear spectrum, it does not necessarily imply actual star formation as emission could arise from another physical process (such as AGN; see e.g. S. F. Sánchez [2020](#)). For instance, the host spectrum of AT 2023clx is similar to the Quiescent galaxies (see Fig. [1](#)), but it exhibits

---

[2]Using traditional definition where negative EW refers to emission.
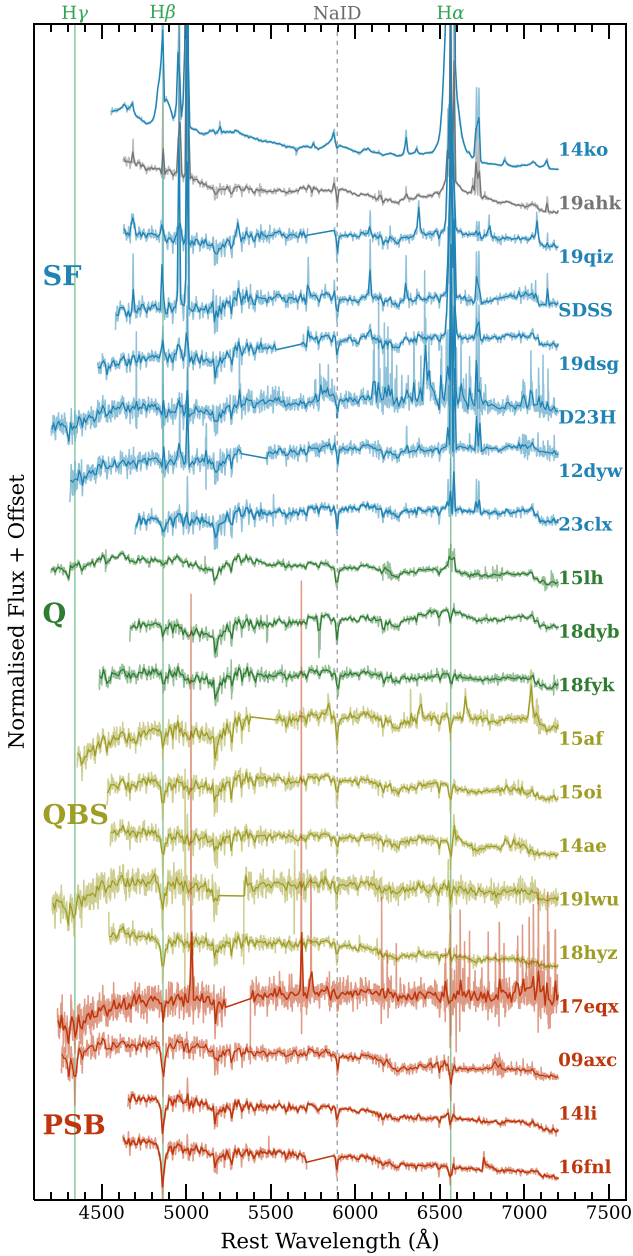
Figure 1. Nuclear spectra of the 20 TDE host galaxies in our sample (lighter shade) under spectra binned to 10 Å (darker shade). The spectra were extracted with an aperture equal to the FWHM measured for stars in the MUSE cubes (see Table 4). The galaxy types are Star-Forming (SF, first from the top), Quiescent (Q, second), Quiescent, Balmer Strong (QBS, third), and Post-Starburst (PSB, fourth) following K. D. French et al. (2020a). Note that AT 2019ahk is classified as a shocked PSB galaxy (SPOG) despite prominent emission lines.

H α emission due to a low-ionization nuclear emission-line region (LINER) listed in NASA/IPAC Extragalactic Database (NED[3]) and in SIMBAD.[4] The host also shows strong star formation in the spiral arms (see Fig. A1), and we adopt the SF label. Finally, galaxies

[3] ned.ipac.caltech.edu
[4] simbad.u-strasbg.fr

that show both weak Balmer absorption and emission are labelled Quiescent.

The galaxy types demographics of the samples are listed in Table 2. In K. D. French et al. (2020a), ∼ 32 per cent of galaxies were QBS or PSB, ∼ 32 per cent were Quiescent, and ∼ 37 per cent SF galaxies. In our MUSE sample there are eight shared objects with K. D. French et al. (2020a) and for these we adopt their classifications. In addition, further five hosts have been classified in single-object publications in the literature. For the rest, we perform a qualitative classification with visual comparison of the spectra presented in Fig. 1. As the discriminant H δ line lies beyond the wavelength range of MUSE for the whole sample, distinguishing between PSB, QBS, and Q galaxies is not directly possible. We use the H α emission to identify the SF galaxies and H β absorption to loosely classify the PSB, QBS, and Q galaxies. Qualitative assessment has inherent uncertainties, but it is sufficient for our needs to compare sample demographics in broad terms. We find that in our sample 35 per cent (7/20) are SF, 45 per cent (9/20) are QBS/PSB, and 15 per cent (3/20) are Quiescent as shown in Table 1. In addition, the host of AT 2019ahk was classified as a 'Shocked Post-Starburst galaxy' (SPOG) by T. W.-S. Holoien et al. (2019), and we retain their classification. SPOGs exhibit both strong Balmer absorption and emission with line ratios inconsistent with star formation, and instead the emission lines are likely ionized via shocks. In general, such galaxies appear to have star formation histories (SFHs) similar to PSB galaxies, but their stellar populations appear to be younger on average (K. D. French et al. 2018), and they may represent a phase in galaxy transformation before traditionally PSB galaxies (K. Alatalo et al. 2016).

In comparison to K. D. French et al. (2020a), the Quiescent host galaxies appear to be underrepresented in our sample, while QBS/PSB are overrepresented. To investigate this, we tested if the two samples are statistically different using the Fisher's exact test, by comparing each of the three classes (QBS/PSB, Q, and SF) against the rest of the galaxies. We find that in all three cases $p > 0.22$, implying that the samples are not statistically significantly different from each other. However, we note that in the absence of a large, representative TDE host galaxy sample, the exact demographics are uncertain. For instance, E. Hammerstein et al. (2021) find that only 2/19 of their TDE host sample exhibit significant H δ absorption indicative of a QBS/PSB nature, and it is possible that the MUSE sample might be biased towards the QBS/PSB hosts.

We also examined whether the central bulge masses of the MUSE sample are representative of the 40 hosts analysed in P. Ramsden et al. (2025; see also P. Ramsden et al. 2022). As only eight galaxies are common between the samples, we estimated the bulge masses for the MUSE sample following the methodology. Values were derived for 14 systems, as for 6 hosts (LSQ12dyw, ASASSN-14ko, ASASSN15lh, AT2018dyb, AT2018fyk, AT2019ahk) sufficient host photometry needed by the modelling was not found. As shown in Fig. 2, the bulge masses of the MUSE sample are much smaller. The two samples are nominally consistent according to the Kolmogorov–Smirnov test ($p = 0.35$), especially as the MUSE sample is concentrated at much lower redshift in comparison to P. Ramsden et al. (2025) (median $z = 0.047$ versus $z = 0.084$). As such the sample is less biased towards brighter and more distant galaxies, possibly explaining the minor discrepancy.

Finally, we inspected the sample demographics in terms of TDE spectral types. The TDEs can be divided into those that show hydrogen (H), hydrogen and helium (H + He), and only helium (He) following S. Van Velzen et al. (2021). Furthermore, E. Hammerstein et al. (2023a) presented a fourth class of TDEs that exhibit featureless spectra based on a uniformly selected sample of

Table 2. The comparison of the MUSE sample and the K. D. French et al. (2020a) TDE sample in terms of their host galaxy types. Total sample size (n) and the numbers in each galaxy types are shown. The values in parentheses refer to the percentage in the sub-type.

Sample	n	Q	QBS/PSB	SF	SPOG
French	41	13 (32 per cent)	13 (32 per cent)	15 (37 per cent)	0 (0 per cent)
MUSE	20	3 (15 per cent)	9 (22 per cent)	7 (35 per cent)	1 (5 per cent)

Figure 2. Bulge mass and redshift comparison between the MUSE sample and sample of P. Ramsden et al. (2025, hereafter R2025). The MUSE sample concentrates on lower bulge masses and lower redshifts than R2025. The samples are nominally consistent, as the MUSE sample is less biased towards more distant brighter galaxies possibly explaining the minor discrepancy. The median values ($\widetilde{M}_{Bulge}, \widetilde{z}$) of are shown with a solid lines for the MUSE sample and dashed lines for R2025.

30 TDEs from ZTF Phase I operations. Their sample consisted of 13.3 per cent featureless, 10.0 per cent He, 56.7 per cent H + He and 20.0 per cent H TDEs. In our sample, a total of 16 TDEs have spectroscopic classifications in the literature (S. van Velzen et al. 2020; P. Charalampopoulos et al. 2022, 2024; J. Zhu et al. 2023; E. Hammerstein et al. 2023a; W. B. Hoogendam et al. 2024). Note that we have left ASASSN-15lh unclassified due to its unique spectral evolution (see e.g. G. Leloudas et al. 2017), although parts of its evolution mostly resemble the featureless class of E. Hammerstein et al. (2023a). The subset consists of 1 He (6.3 per cent), 10 H+He (62.5 per cent), 5 H (31.3 per cent) TDEs, and no featureless TDEs. In comparison to E. Hammerstein et al. (2023a), the MUSE sample slightly underrepresents the two rarest sub-types, but the sample has roughly the same fractions of H+He and H TDEs. Using Fisher's exact test we verified that the samples can be drawn from the same distribution and p-values of all spectral types are > 0.28, indicating that the samples are not statistically significantly different from each other. As such, we consider the sample representative of TDEs in terms of their spectral types.

3 EXTENDED EMISSION LINE REGIONS

We investigated the presence of extended emission line regions (EELRs) that do not follow the host galaxy morphology by using the [O III] λ5007 emission line. While other emission lines, such as [N II] λ6583, have also been used to identify EELRs (e.g. J. L. Prieto et al. 2016), [O III] was chosen as it has been the strongest EELR emission line identified in TDE host galaxies (i.e. T. Wevers & K. D. French 2024). After visual inspection of the MUSE cubes we identified EELRs in 5 of the 20 TDE host galaxies. Three of them have been analysed in the literature (ASASSN-14li: J. L. Prieto et al. 2016; ASASSN-14ko: M. A. Tucker et al. 2021; iPTF16fnl: T. Wevers & K. D. French 2024), but we report two additional events, ASASSN-14ae and AT2019ahk, where we see evidence of extended emission. For these five MUSE cubes, we ran the H II EXPLORER (S. F. Sánchez et al. 2012) routine, as implemented in the IFUANAL package (J. D. Lyman et al. 2018), on [O III] λ5007 emission line maps to spatially bin the EELRs to quantify the extent and amount of the emission. Line maps were generated by subtracting a linear continuum from an image extracted with 10 Å width centred at λ5007. While the approach does not utilize a full stellar population modelling as done by PIPE3D (e.g. S. F. Sánchez et al. 2016), the data-driven continuum subtraction should provide comparable results. False-colour images highlighting [O III] and H α emission are shown alongside grey-scale images of the identified bins in Figs A2 and A3. The extracted spectra corresponding to the bins are shown in Figs A4 and A5.

To characterize the line luminosity, the spectra of the bins were fit for the [O III] emission line in each bin with a simple Gaussian model with FWHM = 170 km s^{-1} as measured from the MUSE line-spread function shown in A. Guérou et al. (2017). The flux limit of the line emission is set very low in the binning routine to thoroughly investigate regions with low level emission. The choice resulted in a number of bins where no real emission line was detected, which were excluded by setting a strict detection limit of 5σ, measured as the ratio of the Gaussian peak luminosity and the standard deviation of the residual in the fitting interval. Note that as we were solely interested in extended regions of emission, we excluded any bins identified within the half-light radius of the host of ASASSN-14ko and AT 2019ahk where significant nuclear line emission is present. The details of the identified bins are listed in Table 3 with the number of bins per galaxy and range of their projected offsets and [O III] emission luminosity.

The EELRs are exclusively identified in systems that are local ($z <$ 0.045; $D_L <$ 200 Mpc), implying a possible detection bias against distant hosts. To investigate this, we ran the same line-fitting routine on spectra extracted at a visually empty region of the 20 MUSE cubes to estimate the upper limit at which the line emission could have gone unnoticed. Given the redshift range of the sample is very wide (0.0111–0.2326), the MUSE spaxels probe very different physical

Table 3. Details of the identified EELR bins. n states the number of bins identified per galaxy, R the range of projected offset of the bins from the nucleus of the galaxy and L the range of the [O III] $\lambda5007$ emission line luminosities. We also show the minimum required luminosity to ionize the EELRs (L_{ion}), and the estimated integrated nuclear luminosity (L_{nucl}).

TDE	n	R (kpc)	L (10^{38}) (erg s^{-1})	Log(L_{ion}) (erg s^{-1})	Log(L_{nucl}) (erg s^{-1})
14ae	7	0.6–2.4	0.98–9.90	> 41.8	< 41.3
14li	32	0.6–6.9	0.11–6.63	> 42.4	41.3
14ko	66	2.4–22.9	0.53–22.10	> 44.2	43.4
16fnl	53	0.7–7.5	0.09–4.60	> 42.8	40.8
19ahk	65	1.9–6.2	0.17–9.27	> 43.1	42.9

Table 4. FWHMs and the aperture sizes used to estimate the [O III] detection limits. If FWHM was larger than 0.75 kpc, the aperture was set to be FWHM. d denotes the used diameter and n the number of spaxels in the aperture.

TDE	FWHM (arcsec)	FWHM (kpc)	d (arcsec)	d (kpc)	n
D23H-1	1.13	3.51	1.13	3.51	20
PTF09axc	0.82	1.70	0.82	1.70	8
SDSSJ134244	0.82	0.60	1.03	0.75	15
LSQ12dyw	0.95	1.60	0.95	1.60	15
ASASSN-14ae	1.20	1.03	1.20	1.03	24
ASASSN-14ko	0.71	0.59	0.89	0.75	9
ASASSN-14li	0.99	0.41	1.80	0.75	59
iPTF15af	0.81	1.21	0.81	1.21	7
ASASSN-15lh	1.01	3.74	1.01	3.74	15
ASASSN-15oi	0.75	0.71	0.79	0.75	8
iPTF16fnl	0.97	0.32	2.26	0.75	87
AT2017eqx	1.62	3.22	1.62	3.22	44
AT2018dyb	1.83	0.67	2.05	0.75	72
AT2018fyk	1.34	1.53	1.34	1.53	31
AT2018hyz	0.74	0.67	0.83	0.75	7
AT2019ahk	1.61	0.85	1.61	0.85	44
AT2019dsg	0.98	0.96	0.98	0.96	15
AT2019lwu	0.77	1.63	0.77	1.63	8
AT2019qiz	0.71	0.22	2.44	0.75	108
AT2023clx	1.15	0.26	3.29	0.75	196

Figure 3. The [O III] $\lambda5007$ luminosity of the EELR bins identified in the five TDE host galaxies (filled markers), and the 5σ detection limits of each MUSE cube against redshift (open triangles). The brightest EELRs bins should have been seen in all the host galaxies regardless of redshift, but there may be bias against galaxies with lower luminosity EELRs.

scales (0.05–0.74 kpc px^{-1}), even before considering the effect of atmospheric smearing. As emission lines are not present in these spectra, we have adopted a strategy to estimate the limit of emission arising from a circular aperture with $d = 0.75$ kpc, chosen as it is comparable to the size of one spaxel at the highest redshift of the sample. To account for atmospheric smearing, we estimated the full width at half-maximum (FWHM) of the MUSE cubes using stars present in the FoV. If the FWHM was < 0.75 kpc, we used an aperture of the size of the physical scale, but if the FWHM was larger we assumed an aperture equal to the FWHM of the cube. As shown in Table 4, in approximately half of the MUSE cubes the physical size was adopted.

Together with the measured EELR luminosities, we can investigate if the emission seen in these 5 galaxies would have been seen in the other 15 hosts as shown in Fig. 3. Limits are shown as explained above, but for the detected EELRs we have rescaled the luminosities to what would be seen of each individual bin at the aperture size used for the detection limits ($d = 0.75$ kpc). This is
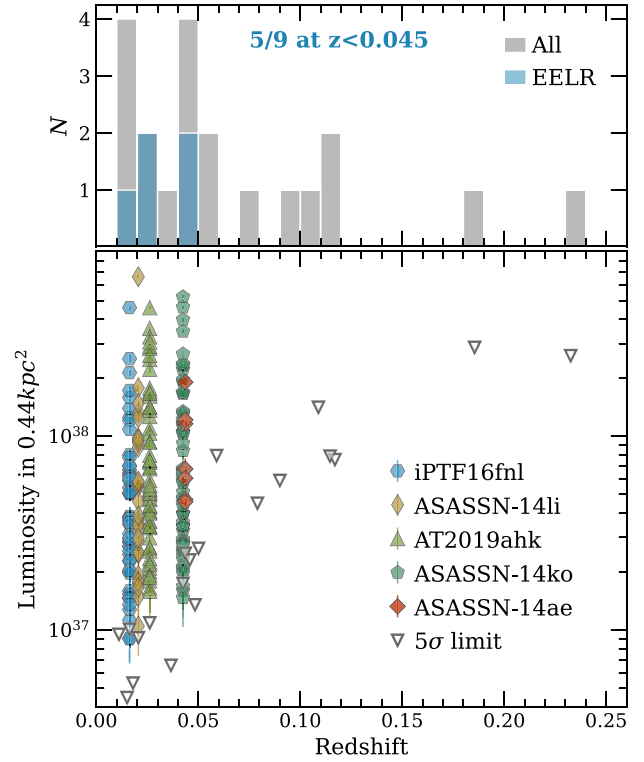
done as a multiplication of average luminosity per spaxel in each bin by the number of spaxels the aperture size would encompass at the redshift of the host. In case the number of spaxels is smaller than covered by the aperture, the average luminosity was multiplied by the actual number of pixels (i.e. luminosity of a bin is not higher than actually measured). The figure shows that the detection limits of the [O III] $\lambda5007$ emission for all hosts are lower than the brightest identified EELRs. In fact, the brightest EELR bins ($\sim 4 \times 10^{38}$ erg s^{-1}) of 4/5 galaxies should have been seen even for the host of ASASSN-15lh at $z = 0.23$, if they were present. However, most of the bins have a significantly lower luminosity (down to $\gtrsim 10^{37}$ erg s^{-1}) and for instance the detections in host of ASASSN-14ae are actually comparable to detection limits of any host above $z > 0.1$. This suggests that low-luminosity EELRs exist in the five hosts and such EELRs can be confidently ruled out only in galaxies below $z \sim 0.05$. Furthermore, it is possible that the physical scales the MUSE spaxels probe at different redshifts also play a significant role. The scale shown in Fig. 3 ($d = 0.75$ kpc; $A = 0.44$ kpc^2) is covered by 101.4 spx at the redshift of iPTF16fnl ($z = 0.0163$) but by 14.9 at the redshift of ASASSN-14ae ($z = 0.0436$), so the pixel size is reduced by factor of 7. At low redshifts it is possible to resolve small-scale EELRs, but as the redshift increases the regions become unresolvable and might therefore be virtually impossible to identify, even if the luminosity was nominally above the non-detection limit for the cube.

3.1 EELR demographics

The galaxies that host EELRs are similar in the fact that they have had significant starbursts in the recent past. The hosts of ASASSN-14li (J. L. Prieto et al. 2016) and iPTF16fnl (T. Wevers & K. D. French 2024) are PSB galaxies and ASASSN-14ae is a QBS galaxy (K. D. French et al. 2016), while the host of AT 2019ahk is consistent with SPOGs (T. W.-S. Holoien et al. 2019). A past starburst has not been verified only for the host of ASASSN-14ko, but the system is a known galaxy merger and it is reasonable to assume that the merger has caused a starburst. Assuming that the QBS/PSB/SPOG galaxies in this MUSE sample are a result of galaxy mergers (e.g. A. I. Zabludoff et al. 1996), 5/11 of the post-merger hosts (including ASASSN-14ko) exhibit EELRs. More significantly, EELRs are identified in all such galaxies at $z < 0.045$, clearly implying a distance bias as discussed above. It is thus possible that EELRs could have been missed in the remaining six QBS/PSB hosts at higher redshift. Two of these galaxies are just outside the redshift range: ASASSN-15oi ($z = 0.0484$) and AT 2018hyz ($z = 0.0458$). To investigate whether EELRs are present, we ran the same procedure to quantify the EELRs in these systems. In both hosts, we identified a single bin at a distance of ~ 5 kpc from the nucleus that showed tentative [O III] emission at $\sim 3\sigma$ level, corresponding to $L \sim 2 \times 10^{37}$ erg s^{-1}. At such a low luminosity, the emission would be well below what was detected in ASASSN-14ae and comparable to the faintest identified bins in the other four systems with EELRs. While faint, the emission is thus on a level expected for EELRs in the TDE hosts in the sample. As there appears to be a distance bias against discovering EELRs in host at $z > 0.045$, we conclude that in the MUSE sample EELRs are present in minimum 45 per cent (5/11) post-merger host galaxies of TDEs. The real fraction is likely higher also because we did not investigate the presence of EELRs deeply embedded in the host galaxies, as was done in Y. Xiong et al. (2025) which identified EELRs near the nuclear region of AT 2019qiz (within 3.7 kpc). If the sample is representative in terms of the host galaxies, the result applies to all TDEs in post-merger hosts. However, as discussed in Section 2.1, the MUSE sample may be biased towards QBS/PSB galaxies and the true occurrence rate is uncertain.

We verified that EELRs are overrepresented in TDE hosts by visually inspecting the host galaxies of a MUSE sample of Type Ia SNe from A. Castrillo et al. (2021). After selecting the galaxies found in the same redshift range as the TDEs, and the ones where the whole galaxy could fit the MUSE FoV, we were left with 46 systems. None of them exhibit EELRs similar to those seen in the TDE host galaxies. While the SN sample is likely not representative of the Ia SN hosts due to selection effects, Type Ia SNe are expected to occur in all types of galaxies, and there should not be a significant bias against ones with EELRs. The lack of EELRs in the Type Ia SN hosts directly implies a low occurrence rate of EELRs in the general galaxy population. As such, incidencies of 25 per cent for the whole sample and 45 per cent for the post-merger TDE hosts, indicate a very significant overrepresentation of EELRs. The result is in agreement with the literature. T. Wevers & K. D. French (2024) suggest that EELRs are overrepresented in PSB galaxies that have hosted TDEs by a factor of ~ 2–5 over a generic galaxy population (e.g. C. López-Cobá et al. 2020; W. C. Keel et al. 2024), and the study determined that 60^{+40}_{-33} per cent of the PSB–TDE galaxies exhibit EELRs. Assuming that the PSB galaxies result from galaxy merger, the study concludes that the post-merger environment is a crucial factor in driving TDE rates. Our study performed on a larger data set agrees with the conclusion.

3.2 The source of ionizing emission

We have verified that at least some of the identified EELRs have to be ionized by nuclear activity using the Baldwin–Philips–Terlevich (BPT; J. A. Baldwin, M. M. Phillips & R. Terlevich 1981) and WHAN diagrams (R. Cid Fernandes et al. 2011). Apart from a few EELR bins for ASASSN-14ko, all of these regions require the ionizing emission to be AGN-like based on the BPT diagram shown in Fig. 4, and star formation can be safely excluded. We also note that as no significant Hα emission is present in the false-colour images in Figs A2 and A3, except for ASASSN-14ko where some star-formation appears to be present along the spiral arm, our focus on the [O III] $\lambda 5007$ emission line to identify EELRs did not bias us against star-forming regions where Balmer emission lines would dominate. Furthermore, the WHAN diagrams shown in Fig. 5, imply that AGN-like hard emission is required to explain the high EW of Hα emission (> 3 Å) with the high [N II] $\lambda 6583$ to Hα ratio. Even in ASASSN-14ae, ASASSN-14li, and iPTF16fnl where some EELRs are found in LINER-like region of the diagram, individual EELRs are located in the AGN regime, where alternative ionizing sources such as post-asymptotic giant branch (post-AGB) stars and low-velocity shocks have difficulties producing the observed line strengths (see e.g. S. F. Sánchez 2020; S. F. Sánchez et al. 2021). While excitation by fast shocks ($v > 200$ km s^{-1}) could result in similar diagnostic line strengths, both J. L. Prieto et al. (2016) and T. Wevers & K. D. French (2024) note that the intrinsically narrow emission line ($v \sim 40$ km s^{-1}) of the EELRs in ASASSN-14li and iPTF16fnl are inconsistent with shocks, favouring the AGN interpretation. Due to the strong Balmer absorption lines present in some of the spectra, the best-fitting simple stellar population STARLIGHT models were subtracted from them before estimating the line fluxes. The details for the models are presented in Section 4.

The BPT and WHAN diagrams imply that a significant level of nuclear activity must have occurred in the recent past for the ionizing emission to reach these EELRs. To investigate whether the current nuclear luminosity is sufficient to light up the EELRs, we estimated the integrated nuclear luminosities using the Hβ and [O III] $\lambda 5007$ emission lines seen in the spectra presented in Fig. 1 using the bolometric correction from H. Netzer (2009), as well as the minimum ionizing luminosity ($L_{\rm ion}$) required by the EELRs following K. D. French et al. (2023). The resulting values are shown in Table 3. The nuclear luminosity of ASASSN-14ae is quoted as an upper limit, due to non-detection of Hβ. Furthermore, we note that the estimates are approximate, and for instance, a more conservative approach using NIR images has resulted in ~ 1 dex higher upper limits for the nuclear luminosities (e.g. T. Wevers & K. D. French 2024).

For ASASSN-14ko and AT 2019ahk the nuclear luminosities appear to be high, but as the MUSE cubes were obtained only ~ 6 months after the TDEs (see Table 1), it is difficult to estimate the actual pre-TDE luminosities. For instance, the nuclear spectrum of AT 2019ahk is visibly blue and exhibits broad emission line wings (see Fig. 1), but the archival host spectrum presented by T. W.-S. Holoien et al. (2019) is red with only narrow lines, implying that a significant level of TDE-related activity remains present in the MUSE cube. The two nuclei are also found on the strong-AGN (sAGN) regime of the WHAN diagrams (Fig. 5), implying hard AGN-like continuum emission. As such, it is plausible that the nuclear luminosity was significantly lower than $L_{\rm ion}$. For the remaining three hosts, the level of nuclear emission is clearly below the luminosity required to ionize the EELRs and the nuclei are located in the LINER-like region of the WHAN diagrams. As noted by T. Wevers & K.
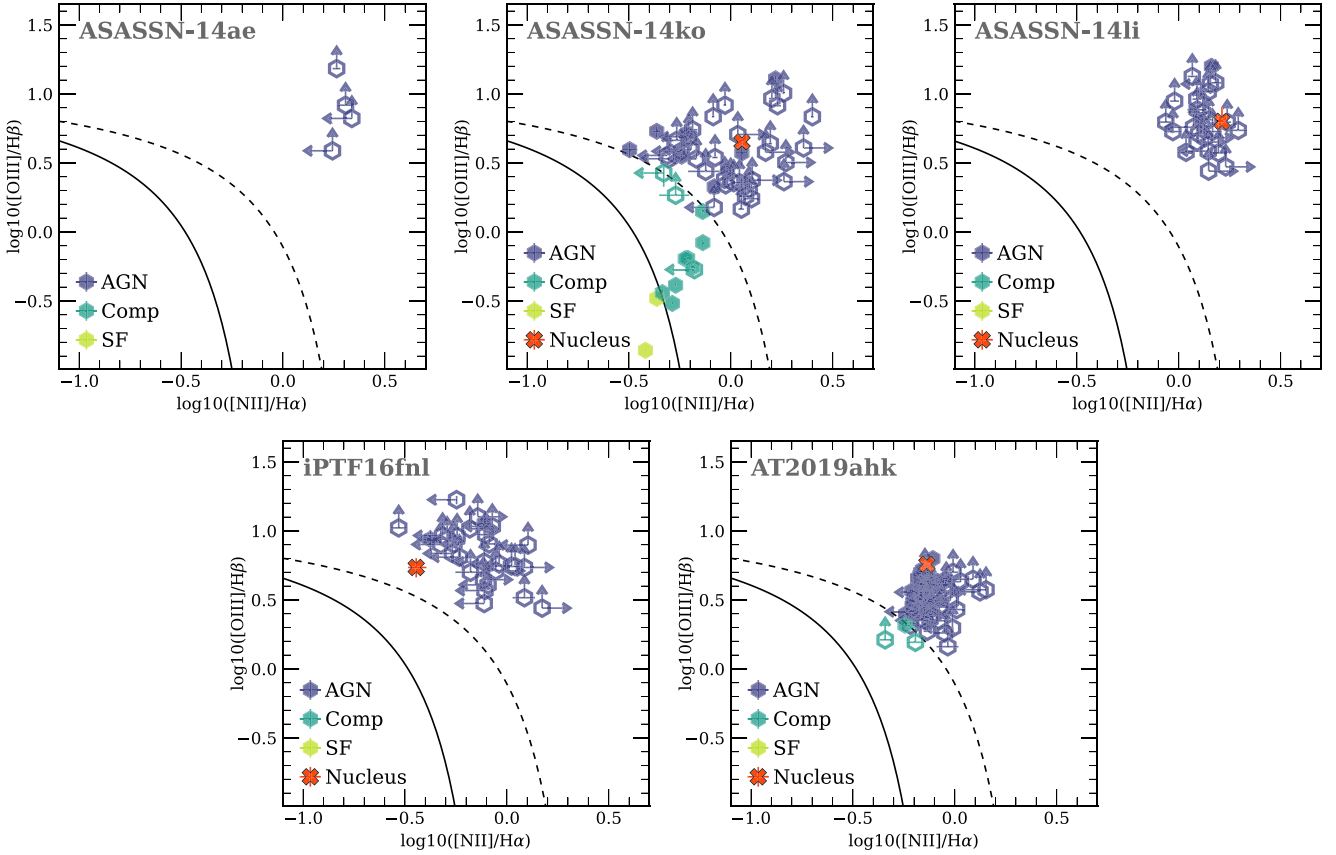
Figure 4. The BPT diagrams for the EELRs and the nuclei of the five TDE host galaxies with detected EELRs. The values are derived from spectra after subtracting the best-fitting STARLIGHT model (see Section 4 for details). Below the solid line, the dominant powering mechanism is assumed to be star formation (G. Kauffmann et al. 2003), while above the dashed line the harder continuum emission (i.e. AGN) is required (L. J. Kewley et al. 2001). Between the two lines, in the composite region, both mechanisms are viable. Bins where both ratios were estimated are marked with solid markers, while limiting values are shown with open markers. In the nuclear spectrum of ASASSN-14ae Hα and Hβ were not detected and [N II] falls on a strong telluric so the value is not shown on the diagram. Note that the few bins where [N II]/Hα could not be estimated are not shown. Except a few bins in ASASSN-14ko, all EELRs require hard AGN continuum.

D. French (2024), this possibly implies higher AGN activity that has since turned off, but past TDEs cannot be ruled out as the cause, even if they would have to be frequent in order to keep the EELRs ionized. As shown by modelling of A. Mummery et al. (2025), galaxies with higher intrinsic rate of TDEs are more likely to show EELRs. With the range of projected offsets of the EELR bins shown in Table 3, we can constrain the time when the nuclei had to be active. Assuming that the projected offsets are the actual light-travel distances, the hard ionizing emission had to be emitted ~ 2000 to ~ 75000 yr before the TDEs. The real values could be higher, but given all five hosts exhibit EELRs at projected offsets $\lesssim 2$ kpc it is likely that there are EELRs at such distances. Given bright AGN phases are predicted to last $\sim 10^4$–10^5 yr (e.g. K. Schawinski et al. 2015; K. D. French et al. 2023), the time-scale in which the AGN would have had to turn off is remarkably short to still power the seen EELRs. Further, it would also be peculiar to see an overrepresentation of TDEs during such a short-lived phase in the galactic evolution, unless there was some causal relation. Following T. Wevers & K. D. French (2024), the results imply that either the AGN turn-off has to be somehow related to the TDEs (or simply the detection efficiency of TDEs), or alternatively the TDE rate in these post-merger galaxies is significant enough for TDEs to provide the required hard emission to power the EELRs.

4 STELLAR POPULATIONS NEAR TO THE SMBHS

We investigate the stellar mass distributions (SMDs) in the near vicinity of the SMBHs by fitting the nuclear spectra (see Fig. 1) with the STARLIGHT spectral synthesis package (R. C. Fernandes et al. 2005; R. Cid Fernandes et al. 2008). STARLIGHT models the observed spectrum (after masking the emission-line-dominated regions and correcting for dust extinction) with a synthetic spectrum created by summing together contributions of simple stellar populations (SSPs). Accumulating the SSPs will provide more realistic SMDs than simply using an initial mass function (IMF) to represent the stellar distribution as it takes into account the evolution of the populations. The results between the two methods would be similar, but with our methodology fewer massive stars, arising from young stellar populations, are present as they explode quickly after formation. On the other hand, low-mass stars are more numerous as they are accumulated from multiple SSPs. In the IFUANAL implementation of STARLIGHT, the SSP base models are taken from G. Bruzual & S. Charlot (2003)[5] as created for the MILES spectral library (P. Sanchez-Blazquez et al. 2006), and use a G. Chabrier (2003)
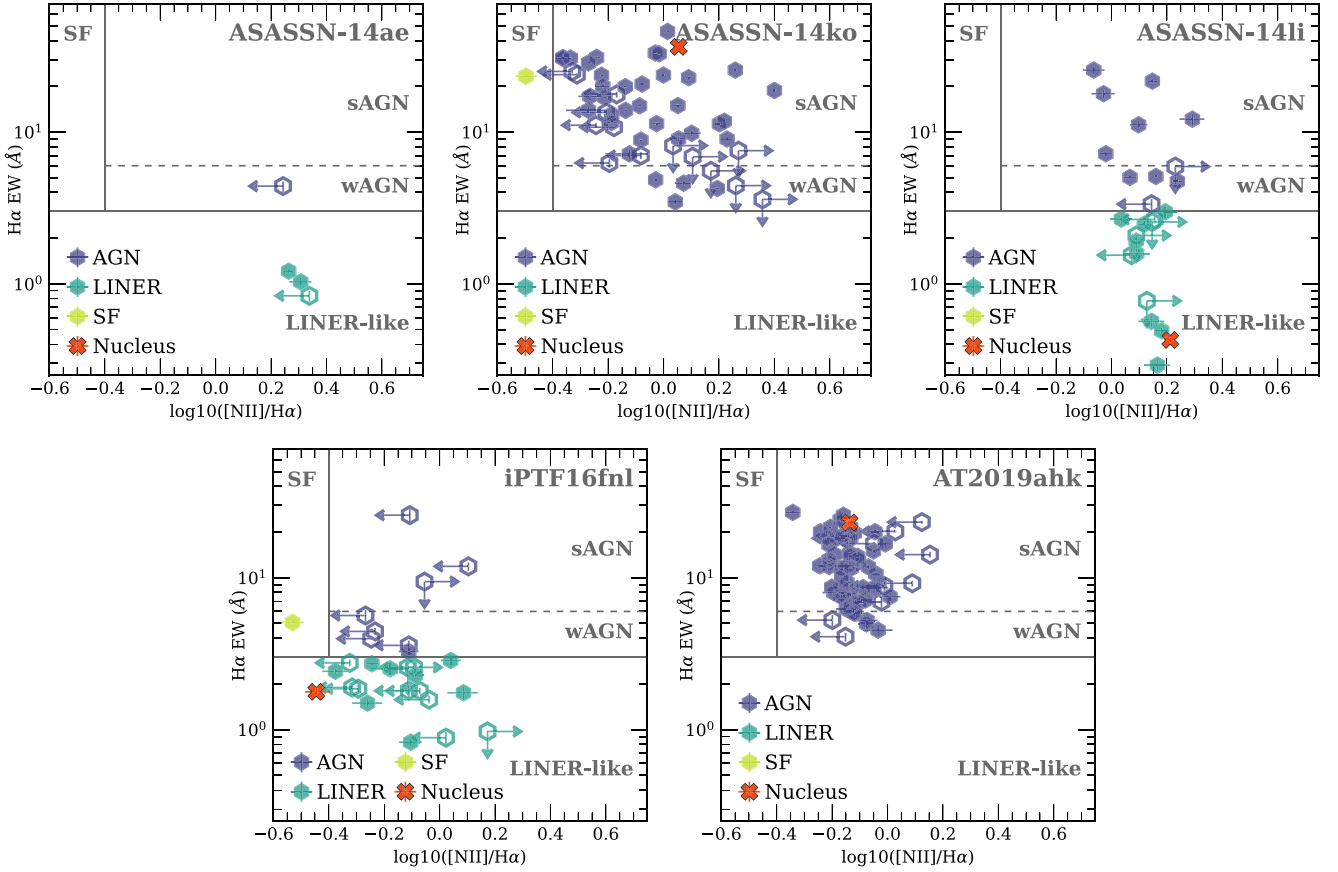
[5] 2016 update at http://www.bruzual.org/bc03/.

Figure 5. The WHAN diagrams (R. Cid Fernandes et al. 2011) of the five TDE hosts that exhibit EELRs. The required ionizing source is divided into star-formation (SF), strong or weak AGN (sAGN, wAGN), or LINER-like based on their H α EW and [N II] to H α ratio. All hosts exhibit some EELRs that require AGN-like ionizing continuum. The nuclear spectra (filled cross) show that ASASSN-14ko and AT 2019ahk are consistent with sAGN, possibly due to the presence of TDE emission in the MUSE cube, while iPTF16fnl and ASASSN-14li are LINER-like. The 3σ upper limit of H α EW for ASASSN-14ae (3.7) effectively places it in LINER-like region, implying that no significant AGN activity is present, but no marker is shown as a strong telluric is located over the [N II] emission.

IMF in the range of 0.1–100 M$_\odot$. The base models are split into 16 ages that range from 1 Myr to 13 Gyr at a roughly logarithmic spacing. We fit for three sets of metallicities ($Z = 0.004, 0.02, 0.05$). However, as the metallicity in the regime from slightly sub-solar to slightly supersolar has only a small effect on the overall SSP age distribution when modelling optical spectra, we focus solely on the ages. While the wavelength range of the MUSE spectra is not blue enough to distinguish between very young populations ($\lesssim 100$ Myr), the nuclear spectra of the TDE galaxies are mostly visibly red (Fig. 1). This implies that the nuclear regions of the galaxies are dominated by old stellar populations, and in lack of young, hot stars, the derived SFHs should be reliable. An example STARLIGHT model is provided in Fig. A6. For more details on the methodology, see J. D. Lyman et al. (2018).

To identify the stellar populations that can produce observable TDEs, we utilize the Hills mass (J. G. Hills 1975): the maximum mass of a non-rotating BH that can disrupt a star outside the event horizon, which is a function of the stellar mass and radius ($M_H \propto R_\star^{1.5} \times m_\star^{-0.5}$). STARLIGHT returns SFHs in the form of light (x_j) and mass fractions (M_j) of the SSPs of different ages, but it does not provide the mass and radius distributions of the actual stars we require. These are not quantities that are readily available from the G.

Bruzual & S. Charlot (2003) models. The mass distribution could be approximated knowing the form of the IMF, and the mass of the stars on the main sequence turn-off at each age, but the stellar radii require an assumption in the form of a mass–radius relation. Instead, we reconstruct them with data from the Binary Population and Spectral Synthesis (BPASS; J. J. Eldridge, R. G. Izzard & C. A. Tout 2008; J. J. Eldridge et al. 2017; E. R. Stanway & J. J. Eldridge 2018) code to investigate the total stellar population seen around the nuclei. The BPASS stellar models are detailed one-dimensional stellar evolution models calculated using a modified version of the Cambridge STARS code. Using the v2.2.1 data release, we extracted the mass (initial and present value), radius and G. Chabrier (2003) IMF weighting for all stellar models at each of the time bins used in the STARLIGHT fits. The BPASS models in the Chabrier IMF variant contain stars ranging from 0.1 to 100 M$_\odot$, roughly logarithmically spaced in mass. Dividing the IMF weighting assigned to each model by its initial mass returns the number of stars of that birth mass which exist within a stellar mass of 10^6 M$_\odot$. Since we only care about the distribution of stellar mass, this scaling value is arbitrary. Taking the radius and the remaining mass of each star at the specified age steps, the corresponding Hills mass can be determined. Note that we calculate the SMDs using only the BPASS single star evolution models, and do not include

Table 5. The adopted black hole masses. The literature values are estimated using M–σ relation based on spectra from high-resolution spectrographs. Where high-quality values were not available, we used the velocity dispersion σ from the STARLIGHT fits to the nuclear MUSE spectra to determine M–σ estimates (AT 2019ahk, LSQ12dyw). Note that for AT 2017eqx and AT 2019lwu the low S/N spectra did not allow estimating σ and in lack of literature M–σ we used black hole masses based on TDE light curve fits. For ASASSN-14ko we adopted the value estimated in A. V. Payne et al. (2021), which is based on several methods.

TDE	$\log M_{\mathrm{BH,lit}}$	$\log M_{\mathrm{BH,MUSE}}$
iPTF16fnl	$5.50^{+0.42}_{-0.42}$ (1)	$6.24^{+0.20}_{-0.20}$
AT2019qiz	$6.52^{+0.34}_{-0.34}$ (2)	$6.50^{+0.18}_{-0.18}$
ASASSN-14ko	$7.86^{+0.31}_{-0.41}$ (3)	$9.05^{+0.09}_{-0.09}$
AT2019ahk	–	$7.78^{+0.10}_{-0.10}$
iPTF15af	$6.88^{+0.38}_{-0.38}$ (1)	$6.88^{+0.16}_{-0.16}$
AT2018hyz	$5.25^{+0.39}_{-0.39}$ (4)	$5.95^{+0.22}_{-0.22}$
ASASSN-14ae	$5.42^{+0.56}_{-0.46}$ (1)	–
AT2023clx	$5.71^{+0.40}_{-0.40}$ (5)	$6.12^{+0.21}_{-0.21}$
ASASSN-14li	$6.23^{+0.39}_{-0.40}$ (1)	$6.51^{+0.18}_{-0.18}$
PTF09axc	$5.68^{+0.48}_{-0.49}$ (1)	$5.11^{+0.27}_{-0.27}$
AT2018dyb	$6.51^{+0.40}_{-0.40}$ (6)	$7.24^{+0.13}_{-0.13}$
ASASSN-15oi	$5.93^{+0.60}_{-0.60}$ (7)	$5.51^{+0.25}_{-0.25}$
AT2019dsg	$6.90^{+0.32}_{-0.32}$ (8)	$6.75^{+0.16}_{-0.16}$
ASASSN-15lh	$8.70^{+0.41}_{-0.40}$ (9)	$8.99^{+0.08}_{-0.08}$
AT2017eqx	6.30 (10)	–
AT2018fyk	$7.69^{+0.39}_{-0.39}$ (7)	$7.72^{+0.10}_{-0.10}$
AT2019lwu	$6.37^{+0.21}_{-0.20}$ (11)	–
LSQ12dyw	–	$5.67^{+0.24}_{-0.24}$
D23H-1	$6.39^{+0.44}_{-0.44}$ (12)	$6.11^{+0.21}_{-0.21}$
SDSSJ134244	$6.06^{+0.51}_{-0.52}$ (12)	$6.28^{+0.20}_{-0.20}$

References: (1) T. Wevers et al. (2017), (2) M. Nicholl et al. (2020), (3) A. V. Payne et al. (2021), (4) P. Short et al. (2020), (5) P. Charalampopoulos et al. (2024), (6) G. Leloudas et al. (2019), (7) T. Wevers (2020), (8) Y. Yao et al. (2023), (9) T. Krühler et al. (2018), (10) M. Nicholl et al. (2019), (11) E. Hammerstein et al. (2023a), (12) K. D. French et al. (2020a).

BPASS binary star models for this calculation. Binary evolution will broaden the mass distribution of living stars at a given age, but for old stellar populations comprising almost exclusively low-mass stars with a relatively low binary fraction ($\sim$25–30 per cent; M. Moe & R. D. Stefano 2017), the impact should only have a small effect on the SMDs which do not change the overall conclusions. At 1.4 Gyr (approximate median age of the youngest stellar populations in the galaxy sample; see Fig. 7) the number of stars with $M > 0.3 \, M_\odot$ is marginally higher in the model that includes stellar binaries. For example, the number ratio $N_{0.5}/N_{0.1}$ increases by $\sim$ 11 per cent, while $N_{1.5}/N_{0.1}$ by about 2 per cent if binaries are included, highlighting that the impact of binary star models is limited for this analysis.

The sub-population of stars that can produce a visible TDE can then be determined by comparing the Hills masses to the SMBH masses mostly collected from literature, shown in Table 5. Most of these values are based on the M–σ relation, where the BH mass is estimated from the velocity dispersion σ of the spectral lines in

high-resolution spectra. In the absence of more reliable values, the BH masses for AT 2019ahk and LSQ12dyw were estimated based on the STARLIGHT fits to the nuclear MUSE spectra using the M–σ relation presented in J. Kormendy & L. C. Ho (2013). As shown in Table 5, the MUSE estimates are in general consistent with those from the literature, and the two values should be reliable. For AT 2017eqx and AT 2019lwu STARLIGHT fits did not converge on a solution of σ due to low S/N spectra, and we used literature values derived from light curve fits. In the case of ASASSN-14ko we adopted the value estimated by A. V. Payne et al. (2021) based on several scaling relations.

The total stellar mass distributions together with the sub-population that can generate an observable TDE are shown in Fig. 6. Given that most BHs are low mass in the context of SMBHs ($\lesssim 10^7 \, M_\odot$), the likeliest stars to create an observable TDE are $0.1 M_\odot$ for the majority of host galaxies. For these galaxies, all the stars in the BPASS models can create a visible TDE. Such low-mass stars completely dominate the population by numbers and in comparison the $1 \, M_\odot$ stars are only a few percent. The only clear exceptions are the hosts of ASSASSN-14ko, ASASSN-15lh, AT 2018fyk, and AT 2019ahk where the BH masses are sufficient to exclude low-mass stars. Interestingly, three of these TDEs exhibit multipeaked light curves. ASASSN-14ko is a known repeating source (e.g. A. V. Payne et al. 2021), while ASASSN-15lh (e.g. G. Leloudas et al. 2017) and AT 2018fyk (T. Wevers et al. 2019, 2023; D. Pasham et al. 2024; S. Wen et al. 2024) show pronounced secondary peaks in the UV. The relation possibly implies that multipeaked light curves may be related to the high BH mass and/or the repeated partial disruptions of higher mass stars. However, even for them TDEs from low-mass stars are possible, as the Hills mass increases if one assumes significant BH spin. This is perfectly exemplified by ASASSN-15lh. G. Leloudas et al. (2017) argues that the event is a TDE, but due to the extreme SMBH ($10^{8.7} \, M_\odot$), only a rapidly rotating BH would sufficiently increase the Hills mass to allow a TDE of a star likely present in the passive environment to occur. Our SMDs support a similar conclusion. The only stars that do not violate their Hills masses have reached the giant phase, and their stellar radii are sufficiently high to allow an observable TDE. However, as these stars are at a particular evolutionary stage, they are very rare in comparison to the whole SMD, and a TDE from a rotating BH is more likely.

The SMDs also allow to investigate the sample properties of the stellar populations. One of the key features, directly related to the massive stars, is the age of the youngest SSP in the fits. Based on the distribution shown in Fig. 7, the Age$_{\mathrm{min}}$ clusters around $\sim$ 1 Gyr, implying absence of stars more massive than $\sim$ 2–3 $M_\odot$ in the nuclear regions of the TDE hosts. However, we note that the fits may not capture the full stellar diversity, and some individual more massive stars are possible present in the near vicinity of the SMBHs. Regardless, their number should be very small, and TDEs from such progenitors should be rare unless there is a mechanism that would overenhance the massive star TDE rate. Possible mechanisms are discussed in Section 4.2.

Finally, we note that we have decided to exclude the youngest 0.5 per cent stellar population in mass. STARLIGHT has a tendency of finding a small amount of young stellar populations ($10^6 - 10^7$ yr), that appear inconsistent with otherwise very old populations. This is likely caused by the fact that many of the cubes are taken soon after the TDE, and some residual blue emission from the TDE itself is likely present in the nuclear spectra (like AT 2019ahk discussed in Section 3), mimicking the effect of young populations. Further, in some cases the S/N of the spectra are quite low, resulting in less
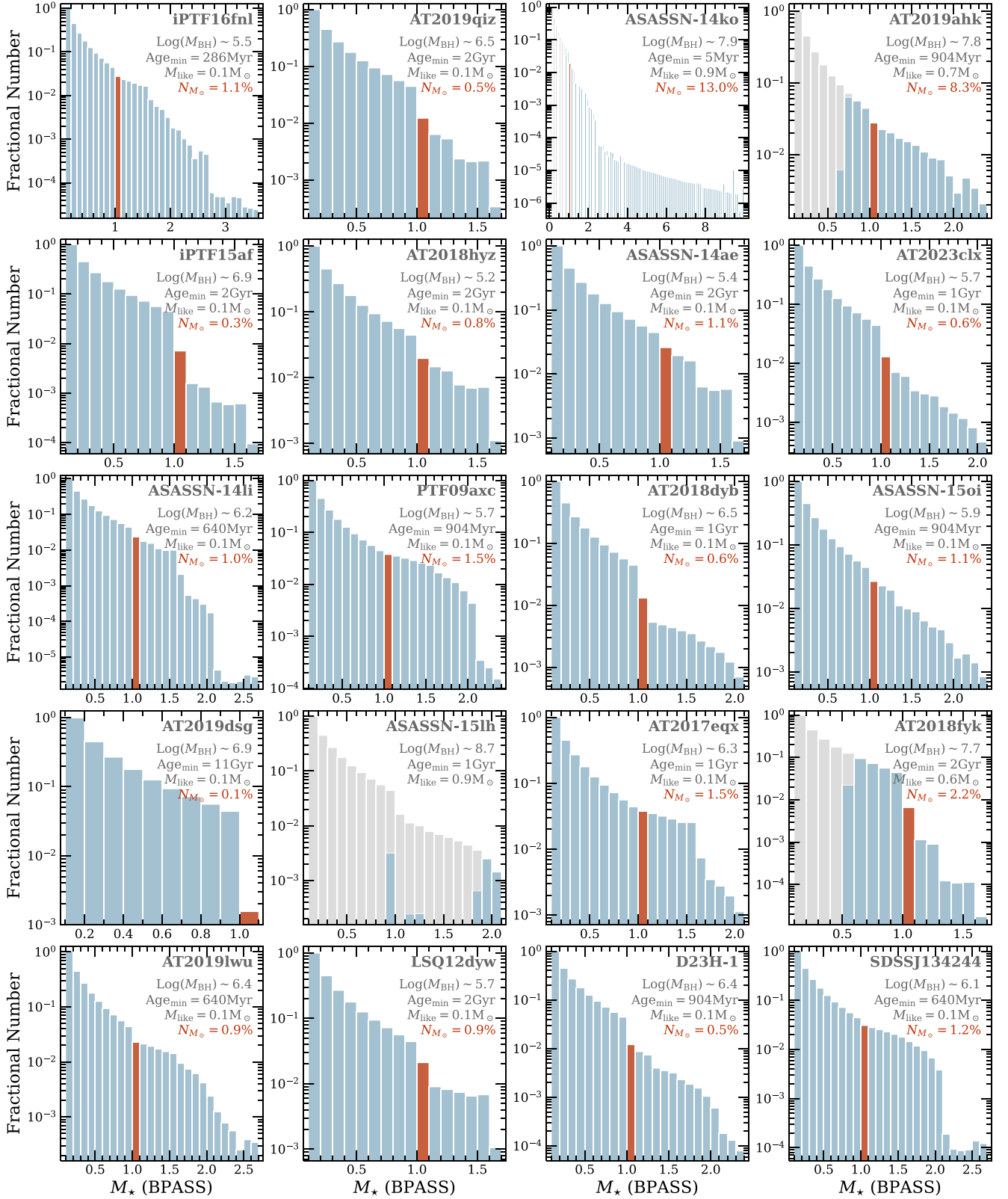
Figure 6. The total stellar mass distributions (SMDs) in the nuclear regions of the galaxies based on STARLIGHT SFHs and BPASS SMDs of individual sub-populations (lighter shade). The population of stars that can generate visible TDEs are highlighted (darker shade). Stars in the $1.0 - 1.1\,M_\odot$ bin are highlighted. Key details such as BH mass, youngest stellar populations, likeliest mass to be disrupted as well as the number density of $1\,M_\odot$ stars that can create a visible TDE are shown. Apart from the few galaxies with very massive BHs ($M_{BH} \gtrsim 10^8\,M_\odot$), the stellar populations that can create a visible TDE are dominated by sub-solar-mass stars. The distribution of ASASSN-15lh is noticeably different due to the high SMBH mass prohibiting the production of visible TDEs for all stars except the small sub-population that have reached the giant phase in the BPASS models, increasing the stellar radii sufficiently to allow an observable TDE.

Figure 7. The logarithmic distribution of identified youngest stellar populations (Age_{min}) in the nuclear regions of the TDE host galaxies. The distribution peaks sharply at ~ 1 Gyr. The median of the distibution ($\widetilde{Age_{min}}$) is shown with the 1σ percentiles, together with mean and standard deviation of a Gaussian fit ($\overline{Age_{min}}$).

reliable fits. While we cannot determine if some of these populations are not real, we consider them likely spurious. Were they included they would increase the maximum mass of stars in the SMDs, but these stars would be extremely rare.

4.1 Comparison to masses of the disrupted stars derived from light-curve models

We can now compare the derived SMDs with the masses of the disrupted stars identified for the TDEs with light-curve modelling. The commonly used light curve fitting routines are MOSFIT (J. Guillochon et al. 2018), TDEMASS (T. Ryu et al. 2020a), and REDBACK (N. Sarin et al. 2024), all of which assume different mechanisms for powering the light curve. MOSFIT generates the light curves by assuming that the rate of energy production follows the fallback rate of the material on the BH at a constant conversion efficiency (B. Mockler et al. 2019), TDEMASS adopts intersection of the debris streams (e.g. T. Piran et al. 2015; Y.-F. Jiang, J. Guillochon & A. Loeb 2016) as the powering mechanism, while REDBACK relies on a cooling envelope model, where the debris forms a pressure supported envelope that powers the UV/optical light curve (N. Sarin & B. D. Metzger 2024).

As shown in Fig. 8, the estimated values are broadly in agreement with the range of allowed masses. However, apart from some models at $\sim 0.1\,M_\odot$, the fit values are mostly found at $\sim 1\,M_\odot$ or above, where our SMDs predict only a fractional amount of stars if any. Further, clear model-specific tendencies can also be identified. MOSFIT is the most used in the literature, and the large number of fits appear to cluster around 0.1, and $1\,M_\odot$. The peak at $\sim 0.1\,M_\odot$ is in line with the SMDs, but the feature is enhanced due to the MOSFIT model set-up. The radii of stars below $0.1\,M_\odot$ are constant in the model, and as a consequence stellar masses of $\sim 0.1\,M_\odot$ are favoured for fast-rising TDEs (for details see B. Mockler et al.
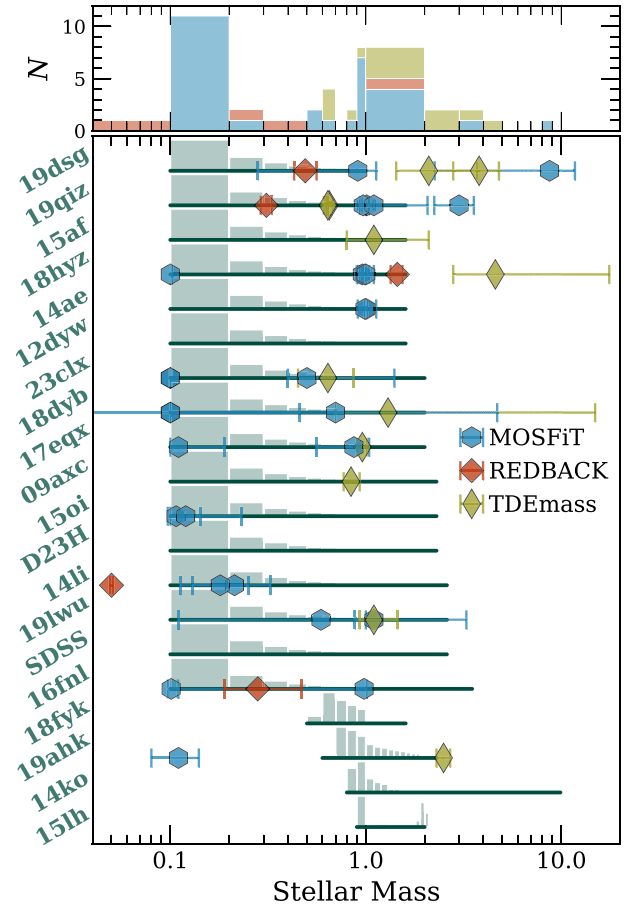

Figure 8. *Bottom:* the allowed mass ranges of the disrupted stars for each TDE (solid line) based on the SMDs shown with histograms (as in Fig. 6). Stellar mass estimates from light-curve models collected from literature are shown. The values are broadly in agreement with the allowed masses, but they are concentrated at higher values than predicted by the SMDs. Stellar populations that violated the Hills mass are excluded. *Top:* the number of models per bin, where the bins have width $0.1\,M_\odot$ at $< 1\,M_\odot$, and $1\,M_\odot$ at $> 1\,M_\odot$. The stellar masses estimated with TDE light curves are collected from the following papers: G. Leloudas et al. (2019), B. Mockler, J. Guillochon & E. Ramirez-Ruiz (2019), M. Nicholl et al. (2019, 2020, 2022), S. Gomez et al. (2020), T. W.-S. Holoien et al. (2020), T. Hung et al. (2020), T. Ryu, J. Krolik & T. Piran (2020a), P. Charalampopoulos et al. (2024), E. Hammerstein et al. (2023a), W. B. Hoogendam et al. (2024), N. Sarin & B. D. Metzger (2024), and S. Zhong et al. (2024).

2019). The latter cluster, however, is inconsistent with the SMDs. It is possibly an artefact of the fitting routine itself, as the polytropic index to define the stellar structure in the MOSFIT model changes at $1\,M_\odot$. On the other hand, TDEMASS finds only relatively high stellar masses (0.7–$5.0\,M_\odot$), clearly at odds with the predictions from the SMDs. Finally, for REDBACK there are fewer publicly available fit parameters, and comparison is difficult, but the few values are evenly distributed between 0.05 and $2\,M_\odot$.

4.2 Causes for the apparent tension

The apparent tension between the masses of the disrupted stars based on the light curve models and the derived SMDs can be a result of a number of different causes. First, it is possible that light curve models have difficulties in capturing the masses of the disrupted

stars. This is especially likely as the stellar mass is considered a degenerate parameter at least in the MOSFIT model (B. Mockler et al. 2019), and deriving an exact solution might not be realistic. As such, these values should be treated with some caution. It is also possible that TDEs of very low-mass stars are in fact very prominent, but we have a detection bias against them (e.g. M. Nicholl et al. 2022). The TDE luminosity scales according to the fallback rate as $\dot{M} \propto M_\star$ (e.g. J. A. P. Law-Smith et al. 2020; T. Ryu et al. 2020b), while the duration of TDEs is expected to scale as $t \propto M_\star^{-1}$. As such TDEs from low-mass stars are possibly faint and slow-evolving making them more difficult to identify than their brighter, faster evolving cousins arising from disruption of more massive stars. However, we note that disruption of low-mass stars have been suggested for fast-rising TDEs such as AT 2020neh (C. R. Angus et al. 2022) and AT 2023clx (P. Charalampopoulos et al. 2024), and it is unclear how large a fraction of the population might be slow-evolving.

It is also possible that our SMDs do not represent the true stellar mass function near the SMBH. One possibly affecting assumption is the used IMF. We have assumed Chabrier IMF (G. Chabrier 2003), as it predicts fewer low-mass stars than the Kroupa IMF (P. Kroupa 2001), and our choice should thus reduce the number of low-mass stars in comparison. It has also been suggested that the IMF in nuclear regions of galaxies is more top-heavy (see e.g. J. R. Lu et al. 2013). However, sub-solar mass stars will still dominate the distribution regardless, unless their production is very significantly stifled. It is unlikely the case here, as the nuclear regions of our TDE hosts exhibit mostly red spectra as is expected of old stellar populations that are dominated by very low-mass stars. Furthermore, the extracted nuclear spectra may also include a significant contribution from stellar populations in the line of sight (LoS). Although it is difficult to ascertain the amount, we have evaluated the significance qualitatively by comparing the nuclear spectra, that should consists of both the nuclear and LoS populations, against spectra extracted with annuli just outside the nuclei that should probe only stellar populations similar to the LoS. The annuli exhibit significantly lower flux per spaxel than the nuclei, implying that LoS population do not contribute significantly to the nuclear spectra. While their contribution is still present, we consider that the nuclear spectra are dominated by stellar populations near the central region.

While the overall stellar populations in central regions are likely old, we may have missed small-scale nuclear stellar clusters that can contain younger populations of stars than in the larger-scale region probed by the MUSE cubes. Such star clusters are coincident with the nuclei and they are found mostly at sizes $r \lesssim 10\,$pc (e.g. N. Neumayer et al. 2011). In late-type galaxies the stellar clusters are dominated by old (more than a few Gyr; N. Neumayer, A. Seth & T. Böker 2020), low-mass stars, but they also contain stars younger than a Gyr (e.g. J. Rossa et al. 2006), even down to a few 100 Myr (e.g. R. Bender et al. 2005; C. J. Walcher et al. 2005; N. Kacharov et al. 2018). In the early-type galaxies the clusters typically consists of only old ($\gtrsim 1\,$Gyr; e.g. L. Monaco et al. 2009; N. Kacharov et al. 2018) populations, but some have shown substantial amount of younger stars $\lesssim 1\,$Gyr (e.g. C. Spengler et al. 2017). As the measured FWHM of the MUSE cubes are at the smallest $\sim 200\,$pc (see Table 4), nuclear clusters that concentrate on scales smaller than 20 pc are beyond our resolving power. If such clusters existed in the host galaxies, it is possible they house a substantial population of younger, more massive stars than probed by the derived SMDs. In fact, using *HST* images, M. Newsome et al. (2025) identified $\sim 340\,$Myr old starburst within 44 pc of the ASASSN-14li host nucleus, that is younger than

the $\sim 550\,$Myr stellar population found at an offset radius of 88 pc. The minimum age of the stellar population in our STARLIGHT fit is $\sim 640\,$Myr, and our nuclear spectrum is clearly dominated by the more distant older stellar population, and the younger population is diluted by the physical resolution of the MUSE cube. However, as discussed above, it is unlikely that IMF of the clusters would be top-heavy enough for very low-mass stars not to dominate the population.

While low-mass stars should be present in the nuclear star clusters, mass segregation has been hypothesized to enhance the rate of TDEs from of supersolar-mass stars. B. Rom & R. Sari (2025) estimated that TDEs from stars in 1–$3\,M_\odot$ range are enhanced by a factor $\sim M_\star$, and at $\gtrsim 3\,M_\odot$ by a factor ~ 9 independent of the stellar mass. While significant mass segregation can thus be expected, the study concludes that the most likely disrupted stars are still the very low-mass stars that dominate the population. Based on our SMDs, $1\,M_\odot$ stars would have to be enhanced by a factor ~ 100 (depending on the host) over the $0.1\,M_\odot$ stars for them to be equally likely. As this is more than predicted by B. Rom & R. Sari (2025), it is unclear if it can be the only process affecting which stars produce TDEs. Similarly, C. S. Kochanek (2016) investigated the rates of TDEs as function of mass of the disrupted star and the SMBH. The study concludes that at $M_{BH} < 10^{6.5}\,M_\odot$ likeliest TDEs arise from $M_\star \sim 0.1\,M_\odot$, and at M_{BH} in range of $10^{6.5}$–$10^{7.5}\,M_\odot$ the typical TDE is caused by an $M_\star \sim 0.3\,M_\odot$ M-dwarf, although the mass function is reasonably flat below $1\,M_\odot$. Given most of our SMBHs are $< 10^{7.5}\,M_\odot$, the results are directly comparable. While the study predicts fewer TDEs from low-mass stars than our SMDs due to the relatively flat TDE rate below $\sim 0.5\,M_\odot$, the TDEs from such stars are still the likeliest and thus should still dominate the observed distribution.

Observational evidence for the disruption of moderately massive stars (1–$2\,M_\odot$) have also been presented in the literature. B. Mockler et al. (2022) investigated the stellar masses of three TDEs in the MUSE sample (ASASSN-14li, iPTF15af, and iPTF16fnl) using N/C ratio with N III $\lambda 1750$ and C III $\lambda 1980$ emission lines present in the *HST* spectra. Given the strict abundance ratio of N/C ≥ 10 (see C. Yang et al. 2017), they concluded that the TDEs were a result of disruption of stars with $M_\star \gtrsim 1.3\,M_\odot$. Using the Kroupa IMF, the study determined that disruptions of moderately massive stars are overrepresented over the galactic stellar population by a factor $\gtrsim 100$. With our SMDs, we can estimate comparable enhancement factors. Using only stars that can generate visible TDEs, stars of $\geq 1.3\,M_\odot$ require constant factors of a minimum few tens to be equally likely as less-massive stars. However, note that this estimate excludes hosts with massive, $\log(M_{BH} > 7.5)$ SMBHs where the factors are much smaller due to the absence of low-mass stars. For the three systems analysed by B. Mockler et al. (2022), our SMDs imply enhancement factors of ~ 70 (ASASSN-14li), ~ 1200 (iPTF15af), and ~ 30 (iPTF16fnl). As such the suggested enhancement seems broadly comparable to our SMDs as it would make TDE from moderately massive stars the likeliest option for most of the host systems.

In the absence of fully reliable distribution of the disrupted star masses, it is difficult to conclude how much of an effect the discussed mechanisms have. Given the theoretical and observational support, it is likely that supersolar-mass stars contribute significantly to the TDE population through some mechanism of mass segregation. However, our results directly imply that TDEs from low-mass stars should be abundant and even dominate the TDE distribution, unless there is a mechanism that stifles production of low-mass TDEs or hampers their detection significantly.

5 CONCLUSIONS

We have presented a detailed investigation of MUSE data of 20 TDE host galaxies, focusing on two key aspects: the extended emission line regions surrounding the galaxies and stellar mass distributions near the SMBHs. Although collected from multiple programmes, the sample appears to be representative of TDEs in terms of the TDE spectral types, and the sub-set of 16 TDEs with literature classifications are divided into 6.3 per cent He-TDEs, 62.5 per cent of H+He-TDEs, 31.3 per cent H-TDEs. The sample is also statistically consistent with the largest TDE host galaxy compilation (K. D. French et al. 2020a) comprising of 35 per cent 'star-forming' (i.e. strong Hα emission), 45 per cent of QBS/PSB implying a significant, recent (< 1 Gyr) starburst and 15 per cent of Quiescent. However, it is possible that the sample is slightly biased towards QBS/PSB galaxies.

In the first part of the analysis we characterized the population of extended emission line regions seen in the TDEs. We identified EELRs in 5/20 of the host galaxies including two previously unreported systems. The systems are found below $z = 0.045$, indicating a possible distance bias, and low-luminosity EELRs cannot be excluded above this redshift. The EELRs are only identified in systems that have likely undergone a galaxy merger, and all post-merger galaxies below $z = 0.045$ show EELRs (5/11 of the sample). Given the probable distance bias, we conclude that a minimum 45 per cent of post-merger TDEs exhibit EELRs in the sample. If the sample is representative in terms of the TDE host galaxies, the value reflects the occurrence rate for all post-merger TDEs.

In all five hosts, at least some EELRs require a hard AGN-like ionizing continuum to explain the diagnostic line strengths. Assuming the projected offsets are the actual light-travel distances, the ionizing continuum had to be emitted 2000 to 75000 yr before the TDE, clearly indicating that significant nuclear activity had to occur in the galaxies for the EELRs to be ionized. However, in three of the systems the current nuclear luminosity is not high enough to explain the EELRs, and in the remaining two the current nuclear luminosity is likely overestimated due to TDE emission present in the observations. Following T. Wevers & K. D. French (2024), the significant overenhancement of EELRs in post-merger TDE hosts implies that either the turn-off of the AGN phase has to be causally related to the TDEs (or efficient detection of TDEs), or the TDE rate in these galaxies is high enough to provide the ionizing continuum.

In the second part of the analysis we focused on the stellar mass distributions in the near-vicinity of the SMBH, to understand the stellar populations that can produce observable TDEs. Based on STARLIGHT fits of the nuclear spectra, we derive the SFHs as well as the light and mass fractions of the simple stellar populations (SSPs) contributing to the integrated nuclear spectrum. We then used BPASS stellar models, weighted with a Chabrier IMF, to obtain the mass and radius distributions of the stellar populations near the BH. The youngest stellar populations in the host nuclei have typical ages of 1 Gyr ($\log(\mathrm{Age}_{\min}/\mathrm{yr}) = 9.16^{+0.24}_{-0.35}$) and the maximum stellar masses present are typically below 2.0–2.5 M$_\odot$. By computing the Hills masses for the stellar populations, we determined that the population that can be disrupted outside the event horizon of a non-rotating SMBH is dominated by very low-mass stars down to 0.1 M$_\odot$. Only for four TDEs, the host SMBH is massive enough to exclude such stars, but even for them low-mass TDEs are possible if one assumes significant BH spin. Interestingly, three of these TDEs exhibit peculiar multipeaked light curves, possibly due to partial repeating disruptions of more massive stars.

Our SMDs are in tension with stellar masses of the disrupted stars derived using light curve models (J. Guillochon et al. 2018; T. Ryu et al. 2020a; N. Sarin et al. 2024), especially TDEMASS, which assumes that the optical light curve is produced by shock collisions. If the observed TDEs come pre-dominantly from approximately solar-mass stars, then the TDE rate from more massive stars has to be significantly overenhanced (by a factor of ~100), as supported by theoretical predictions for mass stratification (e.g. B. Rom & R. Sari 2025), and by observational constraints (B. Mockler et al. 2022). Alternatively, TDE models have to be revised, at least concerning the determination of the disrupted star masses. Regardless, our SMDs directly imply that TDEs from low-mass stars should be abundant and contribute to a significant fraction of all TDEs. This study represents the most spatially resolved (mostly sub-kpc scales) IFU analysis of TDE host stellar populations to date, highlighting the importance of post-merger, old stellar populations in producing TDEs.

DATA AVAILABILITY

The MUSE data analysed in this manuscript are publicly available in the ESO archive.

REFERENCES

Alatalo K. et al., 2016, ApJSS, 224, 38
Angus C. R. et al., 2022, Nat. Astron., 6, 1452
Arcavi I. et al., 2014, ApJ, 793, 38
Auchettl K., Guillochon J., Ramirez-Ruiz E., 2017, ApJ, 838, 149
Bacon R. et al., 2010, in McLean I. S., Ramsay S. K., Takami H., eds, Proc. SPIE Conf. Ser. Vol. 7735, The MUSE Second-Generation VLT Instrument. SPIE, Bellingham, p. 773508
Baldwin J. A., Phillips M. M., Terlevich R., 1981, PASP, 93, 5
Bellm E. C. et al., 2019, PASP, 131
Bender R. et al., 2005, ApJ, 631, 280
Bruzual G., Charlot S., 2003, MNRAS, 344, 1000
Castrillo A. et al., 2021, MNRAS, 501, 3122
Chabrier G., 2003, PASP, 115, 763
Charalampopoulos P. et al., 2022, A&A, 659, A34

Charalampopoulos P. et al., 2024, A&A, 689, A350

Cid Fernandes R. et al., 2008, Revista Mexicana de Astronomia y Astrofisica: Serie de Conferencias, 35, 127

Cid Fernandes R., Stasińska G., Mateus A., Vale Asari N., 2011, MNRAS, 413, 1687

Dong S. et al., 2016, Science, 351, 257

Dressler A., Gunn J. E., 1983, ApJ, 270, 7

Eldridge J. J., Izzard R. G., Tout C. A., 2008, MNRAS, 384, 1109

Eldridge J. J., Stanway E. R., Xiao L., McClelland L. A., Taylor G., Ng M., Greis S. M., Bray J. C., 2017, PASA, 34, e058

Fernandes R. C., Mateus A., Sodré L., Stasińska G., Gomes J. M., 2005, MNRAS, 358, 363

French K. D., Arcavi I., Zabludoff A., 2016, ApJ, 818, L21

French K. D., Yang Y., Zabludoff A. I., Tremonti C. A., 2018, ApJ, 862, 2

French K. D., Wevers T., Law-Smith J., Graur O., Zabludoff A. I., 2020a, Space Sci. Rev., 216, 32

French K. D., Arcavi I., Zabludoff A. I., Stone N., Hiramatsu D., van Velzen S., McCully C., Jiang N., 2020b, ApJ, 891, 93

French K. D., Earl N., Novack A. B., Pardasani B., Pillai V. R., Tripathi A., Verrico M. E., 2023, ApJ, 950, 153

Galbany L. et al., 2016, MNRAS, 455, 4087

Galbany L. et al., 2018, ApJ, 855, 107

Gomez S. et al., 2020, MNRAS, 497, 1925

Graur O., French K. D., Zahid H. J., Guillochon J., Mandel K. S., Auchettl K., Zabludoff A. I., 2018, ApJ, 853, 39

Guérou A. et al., 2017, A&A, 608, A5

Guillochon J., Nicholl M., Villar V. A., Mockler B., Narayan G., Mandel K. S., Berger E., Williams P. K. G., 2018, ApJSS, 236, 6

Gunn J. E. et al., 2006, AJ, 131, 2332

Hadjiyska E. et al., 2012, in Proc. IAU Symp. S285, New Horizons in Time-Domain Astronomy. p. 324

Hammerstein E. et al., 2021, ApJ, 908, L20

Hammerstein E. et al., 2023a, ApJ, 942, 9

Hammerstein E. et al., 2023b, ApJ, 957, 86

Hills J. G., 1975, Nature, 254, 295

Hinkle J. T. et al., 2021, MNRAS, 500, 1673

Holoien T. W.-S. et al., 2019, ApJ, 883, 111

Holoien T. W.-S. et al., 2020, ApJ, 898, 161

Hoogendam W. B. et al., 2024, MNRAS, 000, 1

Hung T. et al., 2020, ApJ, 903, 31

Jiang Y.-F., Guillochon J., Loeb A., 2016, ApJ, 830, 125

Kacharov N., Neumayer N., Seth A. C., Cappellari M., McDermid R., Jakob Walcher C., Böker T., 2018, MNRAS, 480, 973

Kauffmann G. et al., 2003, MNRAS, 346, 1055

Keel W. C., Moiseev A., Uklein R., Smirnova A., 2024, MNRAS, 530, 1624

Kewley L. J., Dopita M. A., Sutherland R. S., Heisler C. A., Trevena J., 2001, ApJ, 556, 121

Kochanek C. S., 2016, MNRAS, 461, 371

Komossa S., Bade N., 1999, A&A, 343, 775

Kormendy J., Ho L. C., 2013, ARA&A, 51, 511

Kroupa P., 2001, MNRAS, 322, 231

Krühler T. et al., 2018, A&A, 610, A14

Law N. M. et al., 2009, PASP, 121, 1395

Law-Smith J., Ramirez-Ruiz E., Ellison S. L., Foley R. J., 2017, ApJ, 850, 22

Law-Smith J. A. P., Coulter D. A., Guillochon J., Mockler B., Ramirez-Ruiz E., 2020, ApJ, 905, 141

Leloudas G. et al., 2015, MNRAS, 449, 917

Leloudas G. et al., 2017, Nat. Astron., 1, 0002

Leloudas G. et al., 2019, ApJ, 887, 218

Linial I., Quataert E., 2023, MNRAS, 527, 4317

López-Cobá C. et al., 2020, AJ, 159, 167

Lu J. R., Do T., Ghez A. M., Morris M. R., Yelda S., Matthews K., 2013, ApJ, 764, 155

Lunnan R. et al., 2014, ApJ, 787, 138

Lyman J. D. et al., 2018, MNRAS, 473, 1359

Lyman J. D., Galbany L., Sánchez S. F., Anderson J. P., Kuncarayakti H., Prieto J. L., 2020, MNRAS, 495, 992

Masterson M. et al., 2024, ApJ, 961, 211

Mockler B., Guillochon J., Ramirez-Ruiz E., 2019, ApJ, 872, 151

Mockler B., Twum A. A., Auchettl K., Dodd S., French K. D., Law-Smith J. A. P., Ramirez-Ruiz E., 2022, ApJ, 924, 70

Moe M., Stefano R. D., 2017, ApJSS, 230, 15

Monaco L., Saviane I., Perina S., Bellazzini M., Buzzoni A., Federici L., Fusi Pecci F., Galleti S., 2009, A&A, 502, L9

Morrissey P. et al., 2018, ApJ, 864, 93

Mummery A. et al., 2025, MNRAS, 544, 2262

Netzer H., 2009, MNRAS, 399, 1907

Neumayer N., Walcher C. J., Andersen D., Sanchez S. F., Boeker T., Rix H.-W., 2011, ApJ, 413, 1875

Neumayer N., Seth A., Böker T., 2020, A&AR, 28, 1

Newsome M., Arcavi I., French K. D., McCully C., Zabludoff A., Stone N., van Velzen S., Wang T., 2025, ApJ, 994, 200

Nicholl M. et al., 2019, MNRAS, 488, 1878

Nicholl M. et al., 2020, MNRAS, 499, 482

Nicholl M., Lanning D., Ramsden P., Mockler B., Lawrence A., Short P., Ridley E. J., 2022, MNRAS, 515, 5604

Pasham D., Coughlin E. R., Guolo M., Wevers T., Nixon C. J., Hinkle J. T., Bandopadhyay A., 2024, ApJ, 971, L31

Payne A. V. et al., 2021, ApJ, 910, 125

Piran T., Svirski G., Krolik J., Cheng R. M., Shiokawa H., 2015, ApJ, 806, 164

Pessi T. et al., 2023a, A&A, 677, A28

Pessi T., Anderson J. P., Lyman J. D., Prieto J. L., Galbany L., Kochanek C. S., Sánchez S. F., Kuncarayakti H., 2023b, ApJ, 955, L29

Prieto J. L. et al., 2016, ApJ, 830, L32

Ramsden P., Lanning D., Nicholl M., Mcgee S. L., 2022, MNRAS, 515, 1146

Ramsden P., Nicholl M., Mcgee S. L., Mummery A., 2025, MNRAS, 541, 1218 (R2025)

Rom B., Sari R., 2025, ApJ, 991, 146

Rossa J., van der Marel R. P., Böker T., Gerssen J., Ho L. C., Rix H.-W., Shields J. C., Walcher C.-J., 2006, AJ, 132, 1074

Ryu T., Krolik J., Piran T., 2020a, ApJ, 904, 73

Ryu T., Krolik J., Piran T., Noble S. C., 2020b, ApJ, 904, 98

Sánchez S. F., 2020, ARA&A, 58, 99

Sánchez S. F. et al., 2012, A&A, 546, A2

Sánchez S. F. et al., 2016, Rev. Mex. Astron. Astrofis., 52, 21

Sánchez S. F., Walcher C. J., Lopez-Cobá C., Barrera-Ballesteros J. K., Mejía-Narváez A., Espinosa-Ponce C., Camps-Fariña A., 2021, Rev. Mex. Astron. Astrofis., 57, 3

Sanchez-Blazquez P. et al., 2006, MNRAS, 371, 703

Sarin N., Metzger B. D., 2024, ApJ, 961, L19

Sarin N. et al., 2024, MNRAS, 531, 1203

Schawinski K., Koss M., Berney S., Sartori L. F., 2015, MNRAS, 451, 2517

Schlafly E. F., Finkbeiner D. P., 2011, ApJ, 737, 103

Schulze S. et al., 2018, MNRAS, 473, 1258

Shappee B. et al., 2014, AAS Meeting #223, p. 236.03

Short P. et al., 2020, MNRAS, 498, 4119

Singleton A. J., Maund J. R., Sun N.-C., Singleton A. J., Maund J. R., Sun N.-C., 2025, MNRAS, 540, 3204

Spengler C. et al., 2017, ApJ, 849, 55

Stanway E. R., Eldridge J. J., 2018, MNRAS, 479, 75

Stone N. C., Metzger B. D., 2016, MNRAS, 455, 859

Stone N. C., Velzen S. v., 2016, ApJ, 825, L14

Tonry J. L. et al., 2018, PASP, 130, 064505

Tucker M. A. et al., 2021, MNRAS, 506, 6014

Van Velzen S. et al., 2016, Science, 351, 62

Van Velzen S. et al., 2021, ApJ, 908, 4

van Velzen S., Holoien T. W., Onori F., Hung T., Arcavi I., 2020, Space Sci. Rev., 216, 124

Walcher C. J. et al., 2005, ApJ, 618, 237

Wen S. et al., 2024, ApJ, 970, 116

Wevers T., 2020, MNRAS, 497, L1

Wevers T., French K. D., 2024, ApJ, 969, L17

Wevers T., van Velzen S., Jonker P. G., Stone N. C., Hung T., Onori F., Gezari S., Blagorodnova N., 2017, MNRAS, 471, 1694

Wevers T. et al., 2019, MNRAS, 487, 4136

Wevers T. et al., 2023, ApJ, 942, L33

Xiong Y., Jiang N., Pan Z., Hao L., Li Z., 2025, ApJ, 989, 49

Yang C., Wang T., Ferland G. J., Dou L., Zhou H., Jiang N., Sheng Z., 2017, ApJ, 846, 150

Yao Y. et al., 2023, ApJ, 955, L6

Zabludoff A. I., Zaritsky D., Lin H., Tucker D., Hashimoto Y., Shectman S. A., Oemler A., Kirshner R. P., 1996, ApJ, 466, 104

Zauderer B. A. et al., 2011, Nature, 476, 425

Zhong S., Xu X., Chen X., Guo H., Fang Y., Du G., Liu X., Liu X., 2024, Res. Astron. Astrophys., 25, 015017

Zhu J., Jiang N., Wang T., Huang S., Lin Z., Wang Y., Wang J.-G., 2023, ApJ, 952, L35

APPENDIX A: FIGURES

Figure A1. *V R I* false colour images of the TDE host galaxies generated from the MUSE cubes. The images are cropped to the near vicinity of the galaxies.
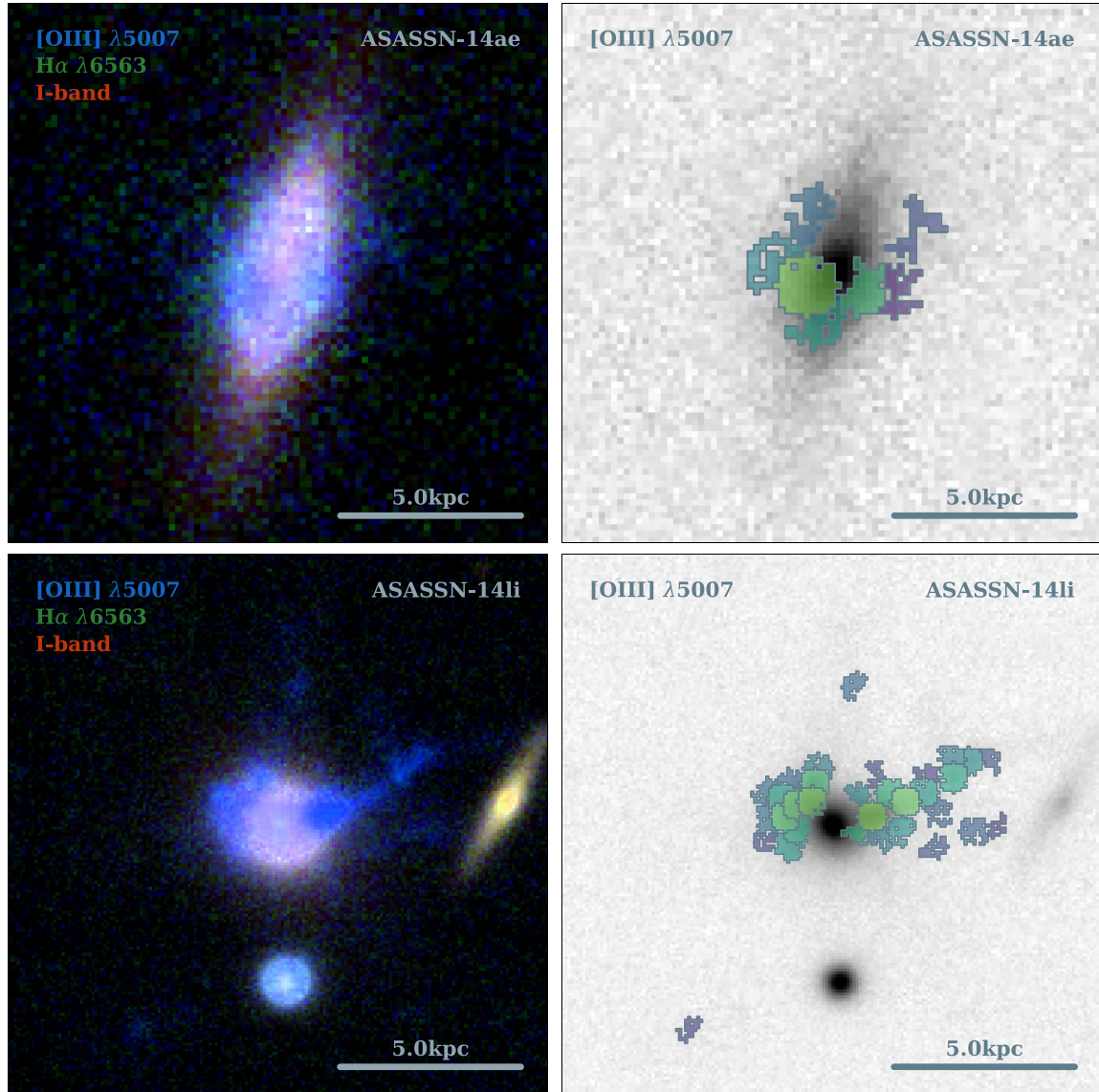
Figure A2. The identified [O III] λ5007 emission line regions for ASASSN-14ae and ASASSN-14li *Left:* false colour image highlighting the [O III] λ5007 (blue) and Hα emission (green). *Right*: identified emission line bins over a greyscale image of [O III] λ5007 emission. The colours refer to the spectra shown in Fig. A4.
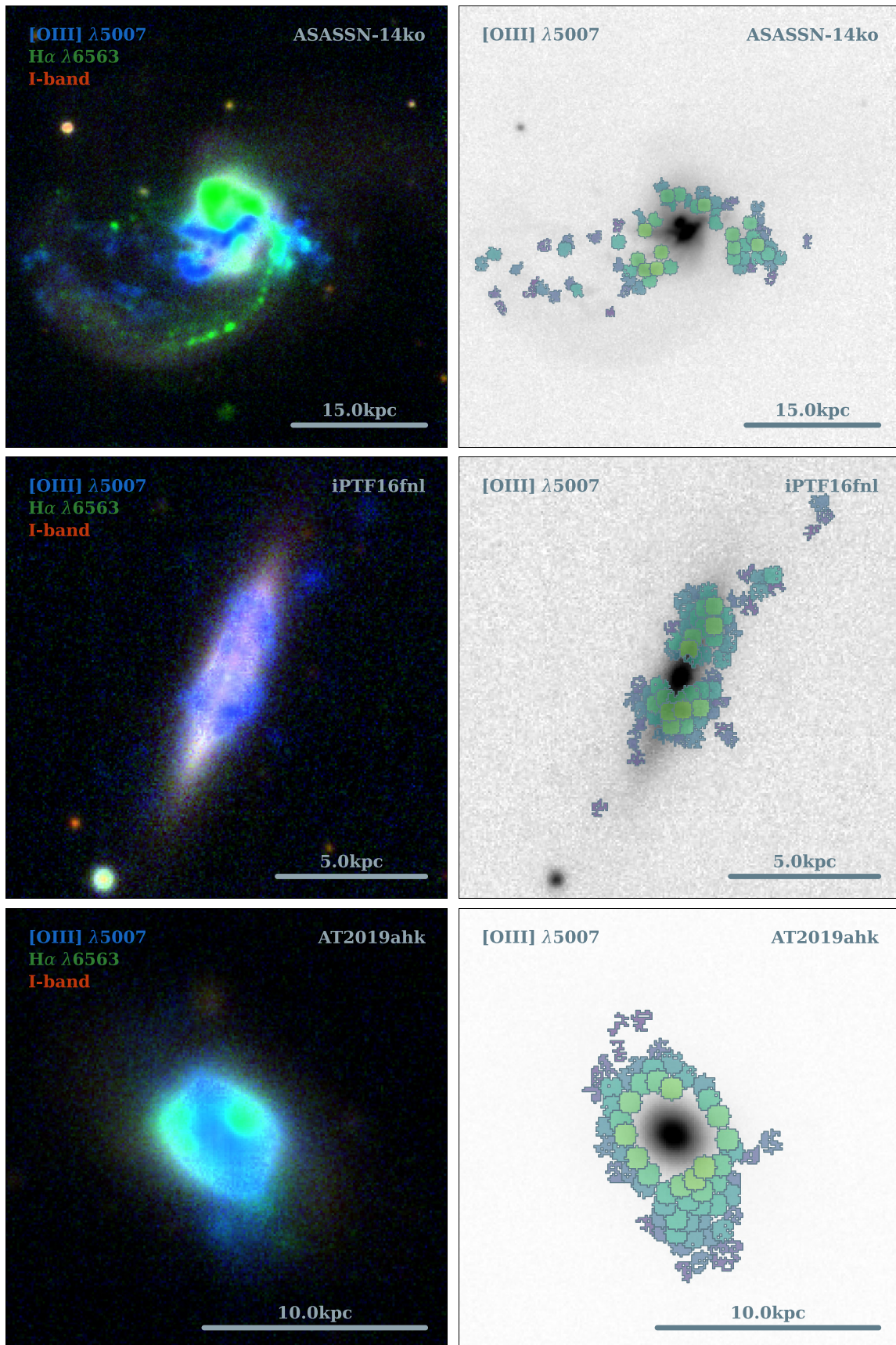
Figure A3. Same as A2 for ASASSN-14ko, iPTF16fnl, and AT 2019ahk. The corresponding spectra are shown in Figs A4 and A5.
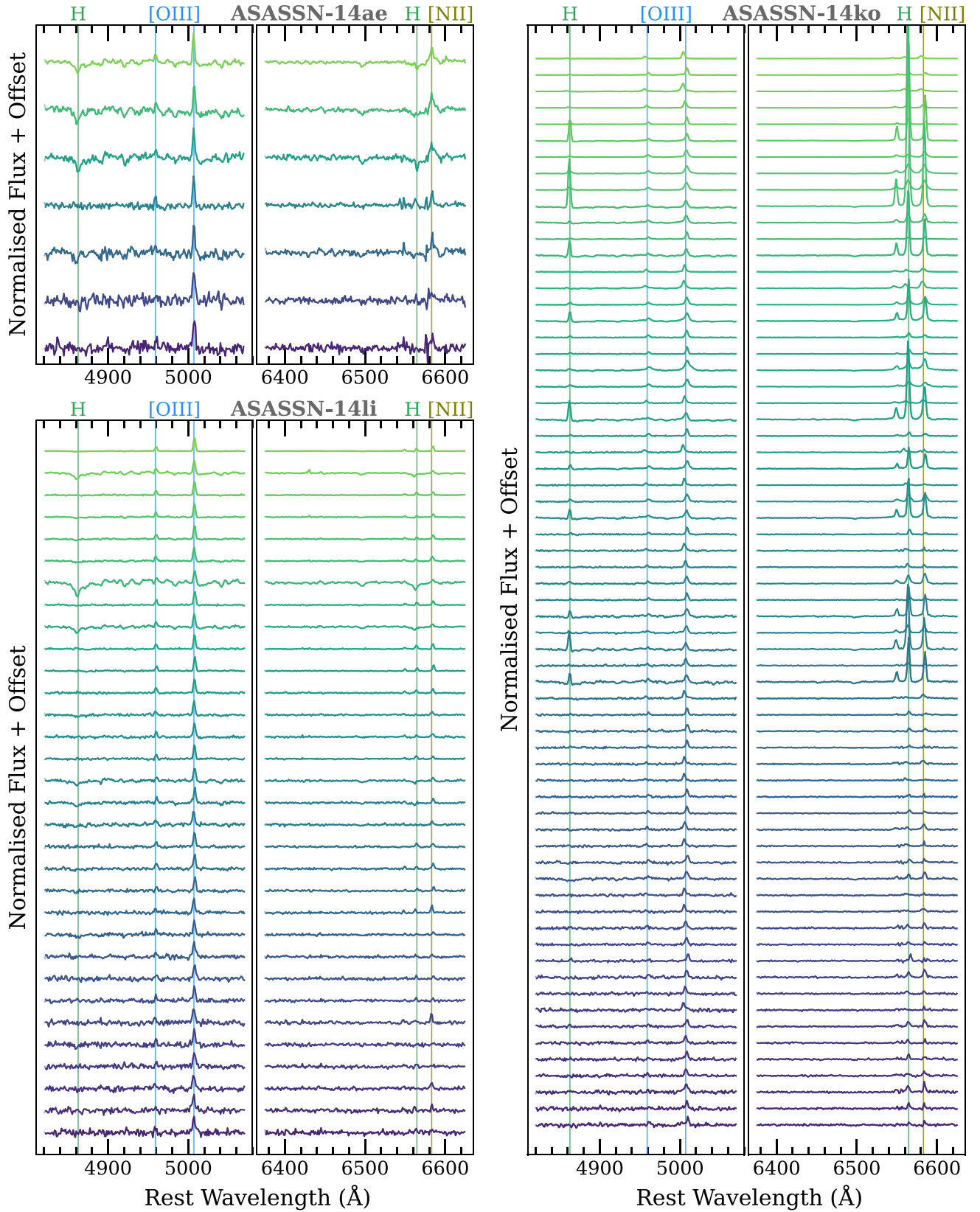
Figure A4. Spectra of the identified emission line bins in ASASSN-14ae, ASASSN-14li, and ASASSN-14ko. The spectra are shown in the order of highest [O III] λ5007 luminosity from top to bottom, and they are normalized by the measured line flux. [O III] λ5007 emission is apparent in all the bins, even if other lines are not identified.

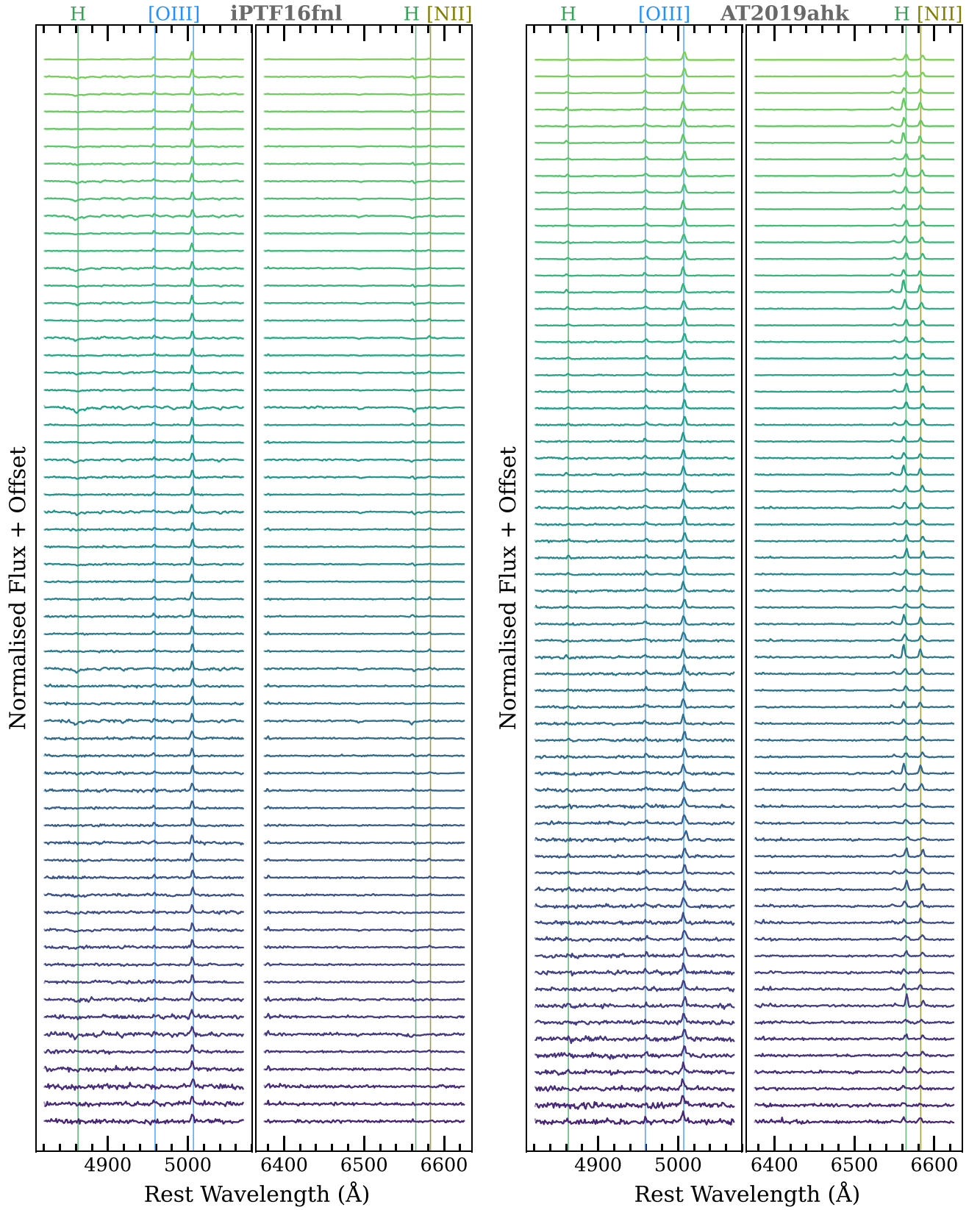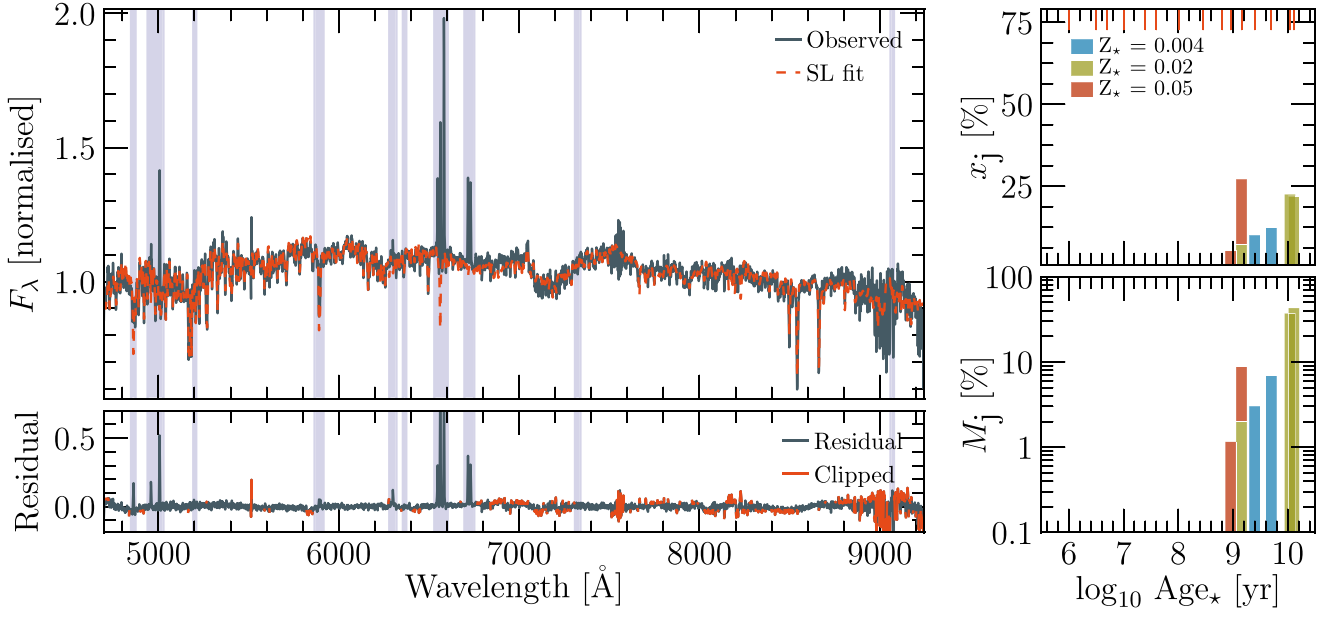**Figure A5.** Same as Fig. A4, but for iPTF16fnl and AT2019ahk.

Figure A6. The best-fitting STARLIGHT model of the nuclear spectrum of the AT 2023clx host galaxy. *Left:* the spectrum, the fit, and the resulting residuals. *Right:* the light (x_j) and mass (M_j) fractions of the different SSPs. Three metallicities were used, but populations were merged into one in the analysis. The regions of strong galaxy lines (shaded) are masked in the fitting routine.

This paper has been typeset from a TEX/LATEX file prepared by the author.